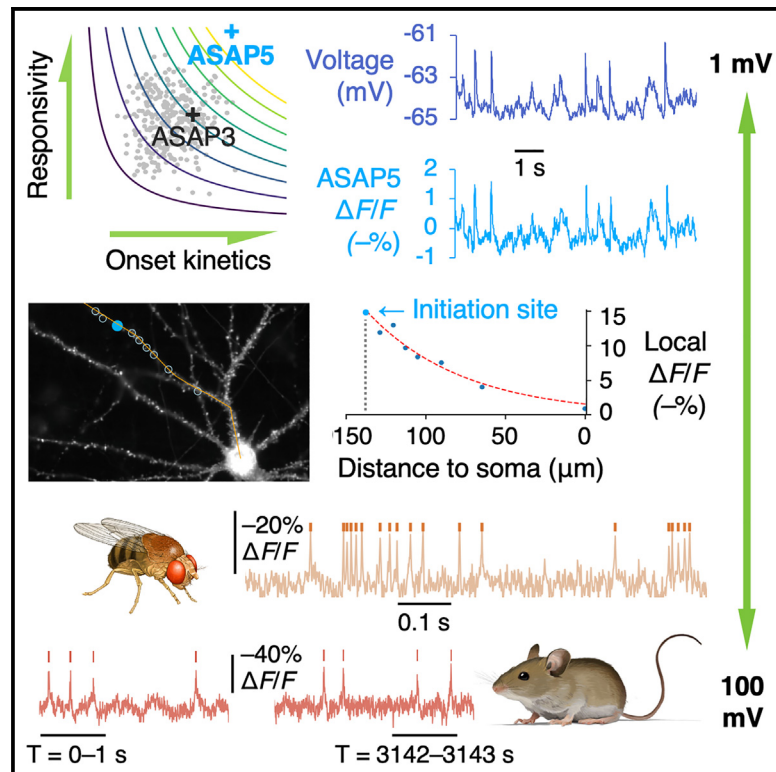


# A fast and responsive voltage indicator with enhanced sensitivity for unitary synaptic events

## Graphical abstract



## Authors

Yukun A. Hao, Sungmoo Lee,  
Richard H. Roth, ..., Thomas C. Südhof,  
Thomas R. Clandinin, Michael Z. Lin

## Correspondence

mzlin@stanford.edu

## In brief

Hao, Lee, et al. report ASAP5, a GEVI that enhances responsivity and accelerates kinetics. It enables single-trial recordings of sub- and suprathreshold activities in flies, mice, and human stem-cell-derived neurons, offering new possibilities to study the dynamics of membrane potentials from 1 to 100 mV.

## Highlights

- Multiparametric screening generated a GEVI with higher gain and faster onset, ASAP5
- ASAP5 exhibits higher responsivity to action potentials and mEPSPs than other GEVs
- ASAP5 reveals mEPSP dendritic propagation and network activity in rat and human neurons
- ASAP5 demonstrated high-SNR voltage recordings in flies, fish, and mice



## NeuroResource

# A fast and responsive voltage indicator with enhanced sensitivity for unitary synaptic events

Yukun A. Hao,<sup>1,2,19</sup> Sungmoo Lee,<sup>2,19</sup> Richard H. Roth,<sup>3</sup> Silvia Natale,<sup>4</sup> Laura Gomez,<sup>5,6</sup> Jiannis Taxidis,<sup>7,17,18</sup> Philipp S. O'Neill,<sup>9,10</sup> Vincent Villette,<sup>11</sup> Jonathan Bradley,<sup>11</sup> Zeguan Wang,<sup>12,13</sup> Dongyun Jiang,<sup>2</sup> Guofeng Zhang,<sup>2</sup> Mengjun Sheng,<sup>3</sup> Di Lu,<sup>3</sup> Edward Boyden,<sup>12,13,14</sup> Igor Delvendahl,<sup>9,10</sup> Peyman Golshani,<sup>7,8</sup> Marius Wernig,<sup>15</sup> Daniel E. Feldman,<sup>5</sup> Na Ji,<sup>5,6</sup> Jun Ding,<sup>3</sup> Thomas C. Südhof,<sup>4,16</sup> Thomas R. Clandinin,<sup>2</sup> and Michael Z. Lin<sup>1,2,20,\*</sup>

<sup>1</sup>Department of Bioengineering, Stanford University, Stanford, CA 94305, USA

<sup>2</sup>Department of Neurobiology, Stanford University, Stanford, CA 94305, USA

<sup>3</sup>Department of Neurosurgery, Stanford University, Stanford, CA 94305, USA

<sup>4</sup>Department of Molecular & Cellular Physiology, Stanford University, Stanford, CA 94305, USA

<sup>5</sup>Department of Molecular and Cell Biology and Helen Wills Neuroscience Institute, University of California Berkeley, Berkeley, CA 94720, USA

<sup>6</sup>Department of Physics, University of California Berkeley, CA 94720, USA

<sup>7</sup>Department of Neurology, UCLA David Geffen School of Medicine, Los Angeles, CA 90095, USA

<sup>8</sup>Semel Institute for Neuroscience and Human Behavior, David Geffen School of Medicine, Los Angeles, CA 90095, USA

<sup>9</sup>Department of Molecular Life Sciences, University of Zurich (UZH), 8057 Zurich, Switzerland

<sup>10</sup>Neuroscience Center Zurich, 8057 Zurich, Switzerland

<sup>11</sup>Institut de Biologie de l'École Normale Supérieure (IBENS), CNRS, INSERM, PSL Research University, Paris 75005, France

<sup>12</sup>Departments of Brain and Cognitive Sciences, Media Arts and Sciences, and Biological Engineering, MIT, Cambridge, MA 02139, USA

<sup>13</sup>McGovern Institute, MIT, Cambridge, MA 02139, USA

<sup>14</sup>Howard Hughes Medical Institute, Cambridge, MA 02139, USA

<sup>15</sup>Department of Pathology, Stanford University, Stanford, CA 94305, USA

<sup>16</sup>Howard Hughes Medical Institute, Stanford University, Stanford, CA 94305, USA

<sup>17</sup>Present address: Department of Physiology, University of Toronto, Toronto, ON M5R0A3, Canada

<sup>18</sup>Present address: Program in Neurosciences & Mental Health, Hospital for Sick Children, Toronto, ON M5G1X8, Canada

<sup>19</sup>These authors contributed equally

<sup>20</sup>Lead contact

\*Correspondence: mzlin@stanford.edu

<https://doi.org/10.1016/j.neuron.2024.08.019>

## SUMMARY

A remaining challenge for genetically encoded voltage indicators (GEVIs) is the reliable detection of excitatory postsynaptic potentials (EPSPs). Here, we developed ASAP5 as a GEVI with enhanced activation kinetics and responsivity near resting membrane potentials for improved detection of both spiking and sub-threshold activity. ASAP5 reported action potentials (APs) *in vivo* with higher signal-to-noise ratios than previous GEVIs and successfully detected graded and subthreshold responses to sensory stimuli in single two-photon trials. In cultured rat or human neurons, somatic ASAP5 reported synaptic events propagating centripetally and could detect ~1-mV EPSPs. By imaging spontaneous EPSPs throughout dendrites, we found that EPSP amplitudes decay exponentially during propagation and that amplitude at the initiation site generally increases with distance from the soma. These results extend the applications of voltage imaging to the quantal response domain, including in human neurons, opening up the possibility of high-throughput, high-content characterization of neuronal dysfunction in disease.

## INTRODUCTION

Neurons process and transmit information by responding to and generating a rich repertoire of transmembrane voltage dynamics. These membrane potential changes are diverse in amplitude and timescale, differ by cell type, and propagate across subcellular compartments. For instance, action potentials (APs) are ~100 mV in amplitude and persist for less than

5 ms.<sup>1</sup> By contrast, the effect of a unitary single synaptic transmission event, which in mammalian excitatory neurons usually entails the release of a single synaptic vesicle, is usually less than 5 mV in amplitude when measured at the cell body but can persist over tens of milliseconds.<sup>2</sup>

In addition to their importance in information processing in the healthy brain, unitary events are also a sensitive sign of synaptic dysfunction in disease.<sup>3,4</sup> When released spontaneously in the



absence of APs, unitary synaptic events are termed miniature excitatory postsynaptic potentials (mEPSPs). Measurement of the frequency of mEPSPs, or the corresponding miniature excitatory postsynaptic currents (mEPSCs), can reveal defects in pre- or postsynaptic function in cultured neurons, including neurons derived from human stem cells.<sup>5–8</sup> However, mEPSP or mEPSC measurements have so far only been possible with patch-clamp electrophysiology, which is inherently low throughput in nature, creating a rate-limiting step in characterizing synaptic effects of disease mutations or in screening for corrective drugs. Thus, recording neuronal populations non-invasively with millivolt resolution and millisecond temporal resolution has been a long-standing goal.

Genetically encoded voltage indicators (GEVIs) have improved dramatically in the last decade, such that single-trial imaging of spikes and subthreshold events is now routine in the mouse brain.<sup>9–16</sup> However, reliable single-trial detection of electrical events has not yet been achieved for mEPSPs. Here, we describe the development of ASAP5, a voltage indicator with faster and steeper fluorescence responses to changes in membrane potential than its predecessors ASAP3.<sup>14</sup> ASAP5 allowed for single-trial two-photon detection of graded and subthreshold events in flies and mice and outperformed previously established GEVIs ASAP3, JEDI-1P,<sup>16</sup> and JEDI-2P<sup>10</sup> in response amplitude and signal-to-noise ratio (SNR) in AP detection under one-photon or two-photon illumination. In cultured rodent neurons, ASAP5 detected single-mV mEPSPs at the cell body with higher responsivity and similar accuracy when compared with Voltron2, a leading opsin-based sensor that requires loading of an exogenous chemical dye.<sup>15</sup> Taking advantage of the superior responsivity of ASAP5 for detecting subthreshold changes in membrane potential, we measured the dendrosomatic propagation of mEPSPs in cultured rodent neurons. These studies revealed that mEPSP amplitude at the synapse scales with distance from the soma and that these distal signals are attenuated more strongly than proximal signals, results that extend previous measurements of dendritic properties using electrophysiological approaches. Thus, ASAP5 improves AP and subthreshold detection in a variety of illumination regimes *in vivo* and expands the scope of voltage imaging to detect quantal synaptic events in culture, including in human stem-cell-derived neurons.

## RESULTS

### Improving ASAP for larger responsivity and faster activation kinetics

We selected ASAP3 as a template for making a GEVI with high responsivity around  $-70$  mV and fast activation kinetics. The fluorescence-voltage conversion of ASAP3 is largest around  $-88$  mV, making it more promising for detecting millivolt-scale events around  $-70$  mV (resting membrane potential) than ASAP4b and ASAP4e, whose most sensitive voltage values are  $0$  and  $30$  mV, respectively. Since the response to voltage transients is a function of both activation kinetics and steady-state response, we designed a multiparametric screening protocol intended to improve both activation kinetics and steady-state response.

To screen for improved sensors, we deployed a platform that can measure changes in sensor fluorescence across a near-instantaneous voltage transition between  $-70$  and  $0$  mV with high temporal resolution as previously described.<sup>9</sup> For fast electrical events such as APs (which have a time to peak of  $\sim 2$  ms) and EPSPs (which have a time to peak of  $\sim 5$  ms), the peak fluorescence change ( $\Delta F_{\text{event}}/F_0$ ) can be related to our screen parameters by the equation  $\Delta F_{\text{event}}/F_0 \approx (\Delta F_{\text{steady}}/F_0) \times c_{\text{fast}}(1 - e^{-t/\tau_{\text{fast}}})$ , where  $\Delta F_{\text{steady}}/F_0$  is the steady-state fluorescence change to a step voltage change of the event amplitude,  $c_{\text{fast}}$  is the fractional contribution of the fastest-rising component and  $\tau_{\text{fast}}$  the fastest time constant in the case of multiexponential activation kinetics, and  $t$  is the time to peak of the voltage transition. For reference, ASAP3 exhibits  $\Delta F_{\text{steady}}/F_0$  of  $-51\%$  for  $100$ -mV depolarizations,  $\tau_{\text{fast}}$  of  $3.7$  ms, and  $c_{\text{fast}}$  of  $81\%$ . ASAP3 responses to AP waveforms *in vitro* are about  $20\%$  at peak, consistent with continued kinetic limitation.<sup>14</sup> To improve responses to fast events, we therefore sought to increase steady-state responsivity, enlarge the contribution of the fast-rising component, and decrease the fast time constant.

We hypothesized that we could improve both responsivity and kinetics by optimizing the interactions between ASAP3 and the surrounding lipid milieu to reduce energetic barriers to moving the S4 voltage-sensing helix (Figure 1A). In previous mutagenesis screens of ASAP3 and ASAP4, we found conservative mutations at T399, I412, F413, and Q414 to modulate voltage tuning and activation kinetics. As these sites are predicted to contact the lipid bilayer, we designed a 324-member library comprising  $9 \times 9$  amino acid (aa) choices at positions F413 and Q414 in combination with T399T/R and I412I/V (Figure 1B). We expressed this library in HEK293T cells expressing the inwardly rectifying potassium channel Kir2.1, which has a resting membrane potential of  $-70$  mV, and implemented software and hardware improvements to enable imaging of electroporation-induced depolarization at  $300$  frames per s (fps, Figure S1A). We then ranked ASAP3 variants by the product of  $\Delta F_{\text{steady}}/F_0$  to capture responsivity and a kinetics index that captured the fraction of the full response that was reached in  $6.66$  ms (corresponding to  $2$  video frames) as an estimation of relative responses to APs (Figure 1C). This process identified ASAP3 I412V F413V Q414R (ASAP3 VVR), as well as ASAP3 I412V F413I Q414R (ASAP3 VIR) (Figure S1B).

In a second round of screening, we separately mutated  $16$  sites that contacted the voltage-sensing S4 helix in ASAP3 VVR to all possible aa, comprising a second library of  $320$  variants (Figures 1A and 1B). This screen identified D145A and D145C as improved variants (Figure S1B). Finally, we recorded from single cells using patch-clamp electrophysiological recordings to test  $8$  combinations of D145A/C and a nearby linker mutation R149K in ASAP3 VVR and ASAP3 VIR. From this final round of screening, the mutant with the largest responses to AP-like waveforms proved to be ASAP3 VIR D145A R149K (Figure 1C; Table S1), which we named ASAP5.

### Characterizing ASAP5 performance for small- and large-amplitude events

We compared ASAP5 in the steepness of the response to the earlier ASAP-family GEVIs ASAP3,<sup>14</sup> JEDI-1P,<sup>16</sup> and

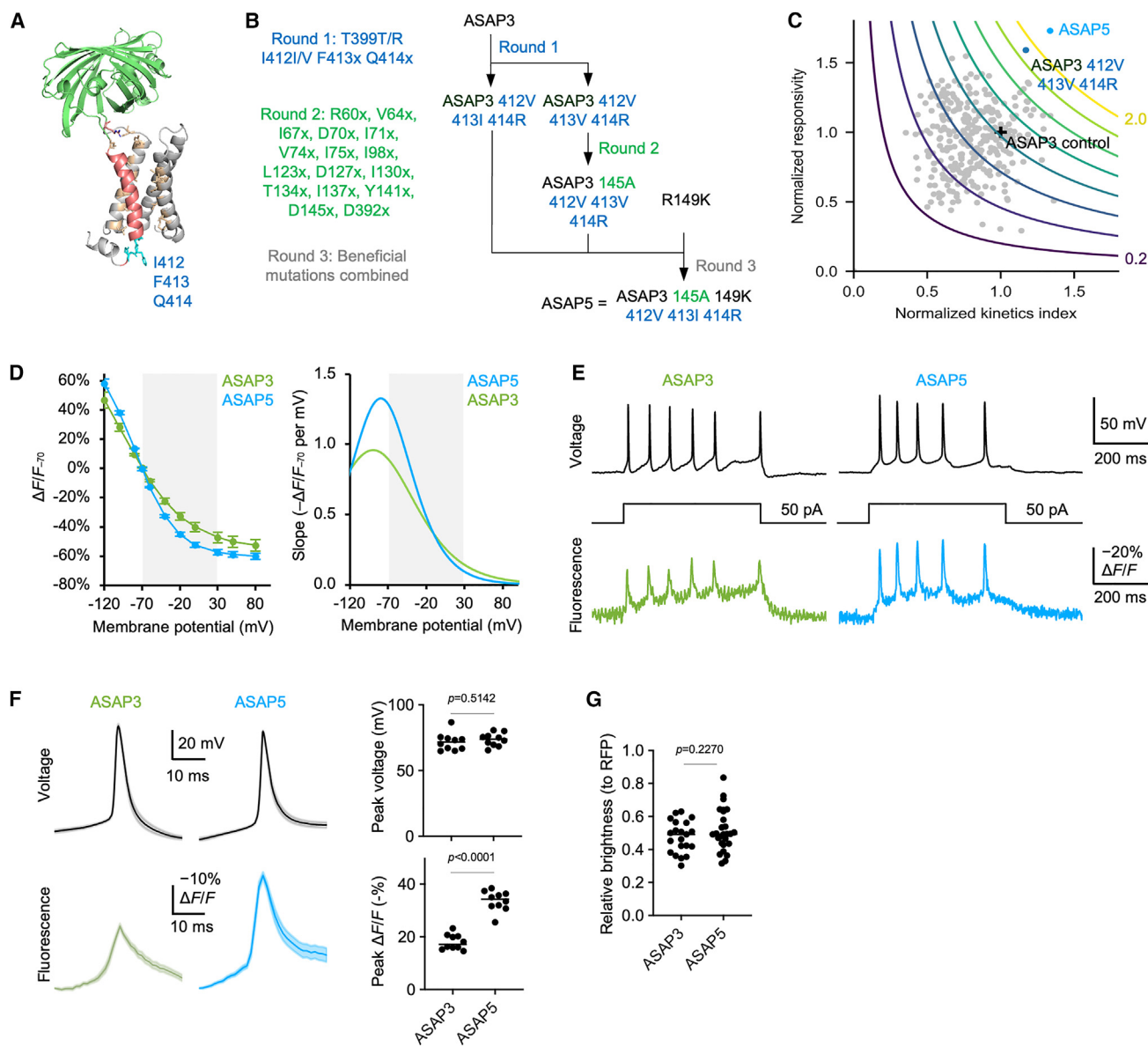


**Figure 1. Protein engineering and biophysical properties of ASAP5**

(A) A structural model of ASAP3 based on homology modeling. The engineered sites are highlighted by sticks representation.

(B) 3 rounds of screening and the engineering pathway from ASAP3 to ASAP5.

(C) Scatter plot for normalized kinetics index and normalized responsivity of variants in the first round of screening. ASAP5 is added for comparison. Colored lines represent the product of the two parameters, ranging from 0.2 to 2.0 with equal distance.

(D) Steady-state fluorescence-voltage (F-V) function normalized to  $-70$  mV (left) and the normalized slope of this function (right). Error bars, standard deviation (SD) of 5, 5 HEK293A cells for ASAP3 and ASAP5, respectively.

(E) Example traces of action potentials induced by current injection in cultured hippocampal neurons expressing ASAP3 (left) or ASAP5 (right), recorded by electrode and camera (800 fps).

(F) Left: averaged voltage and fluorescence waveforms of current-induced spikes in cultured rat hippocampal neurons at room temperature.  $n = 10$  cells, shaded area:  $\pm 1$  SEM. Right: statistical comparison of the peak amplitudes of the voltage and optical spikes. Optical recording was at 800 fps. Welch's t test was used for the two comparisons and  $p$  values are reported.

(G) Relative brightness of GEVI to fused mCyRFP3 in cultured hippocampal neurons.  $n = 21$  and 27 neurons for ASAP3 and ASAP5, respectively. Welch's t test was used for the comparison and  $p$  values are reported.

JEDI-2P.<sup>10</sup> When depolarized from  $-70$  to  $30$  mV, ASAP5 displayed a 57% decrease in fluorescence, representing a 20% improvement in responsivity compared with ASAP3 (Figure 1D; Table S2).

The F-V curve of ASAP5 exhibited a steeper slope at the resting membrane potential of  $-70$  mV than the F-V curve of ASAP3 (Figure 1D), such that the fluorescence-per-voltage

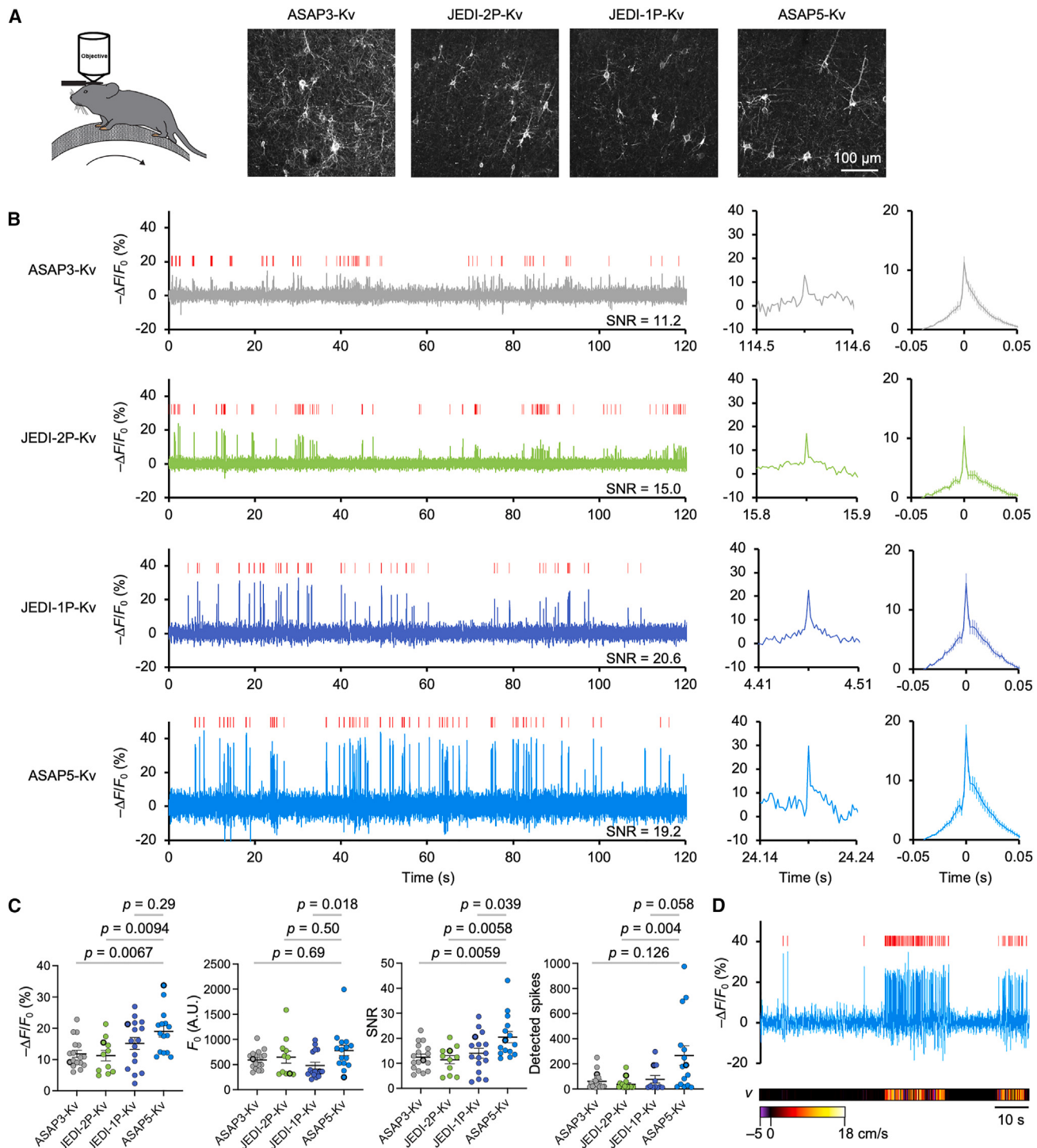


**Figure 2. Comparative performance of ASAP5 *in vivo* under one-photon illumination**

(A) Left: schematic drawing of a head-fixed mouse running on a wheel during *in vivo* voltage imaging. Right: representative post hoc histology images of sparsely labeled CaMKII $\alpha^+$  neurons expressing soma-targeted versions of ASAP3, JEDI-2P, JEDI-1P, and ASAP5.

(B) Left: representative baseline-corrected 2-min 500 fps GEVI recordings. Middle: single-AP examples. Right: average waveform of all detected APs for each GEVI. Error bars, SEM.  $n = 17$  cells from 6 mice for ASAP3-Kv, 16 cells from 4 mice for JEDI-1P-Kv, 11 cells for 5 mice for JEDI-2P-Kv, and 15 cells from 4 mice for ASAP5-Kv.

(legend continued on next page)

conversion ratio was 1.3% per mV, compared with 0.9% for ASAP3, 0.9% for JEDI-1P, and 0.7% for JEDI-2P (Figure S1C). This higher slope is expected to improve detection of subthreshold events such as EPSPs.

We next characterized activation and deactivation kinetics. ASAP5 displayed an activation time constant of 2.61 ms at room temperature with a fractional fast component of 92% and an activation time constant of 0.78 ms with a fractional fast component of 95% at 37°C. Similarly, ASAP5 displayed a deactivation time constant of 4.30 ms with a fractional fast component of 75% at room temperature and 1.12 ms with a fractional fast component of 63% at 37°C (Table S2). ASAP3, JEDI-1P, and JEDI-2P kinetic measurements using the same method revealed that ASAP5 is the fastest member of the ASAP family in both activation and deactivation (Table S2).

We next compared responses of ASAP5 and other ASAP-family GEVs to neuronal activity waveforms. In response to commanded 2-ms AP waveforms, ASAP5 showed approximately 40% larger responses than JEDI-1P or JEDI-2P (Figure S1D). In rat hippocampal neurons injected with current, ASAP5 traces corresponded well to electrical responses for both sub- and suprathreshold components (Figure 1E). Fluorescent responses to current-evoked APs were 2-fold larger in amplitude with ASAP5 than with ASAP3 (Figure 1F). As expected from their similar  $F/F_{max}$  ratios at -70 mV (Figure S1C), ASAP5 and ASAP3 exhibited similar baseline brightness when expressed in cultured neurons (Figure 1G).

#### Comparing ASAP5 performance *in vivo* under one-photon illumination

We tested ASAP5 in awake behaving mice (Figure 2A), comparing it to other GEVs under one-photon illumination. To achieve sparse labeling of neurons in motor cortex, we co-injected CaMKIIα-cre adeno-associated virus (AAV) and cre-dependent AAV expressing ASAP3-Kv, JEDI-1P-Kv, JEDI-2P-Kv, or ASAP5-Kv, where Kv denotes the proximal retention and clustering signal of Kv2.1 for somatic enrichment (Figures 2A and S2A). Imaging through an optical window at 500 fps with a sCMOS camera detected optical spikes with the amplitude and duration expected for APs (Figure 2B; Video S1), with ASAP5-Kv exhibiting significantly higher SNR for AP detection than the other GEVs (Figures 2B and 2C). In some neurons, ASAP5-Kv optical spikes occurred preferentially with running (Figure 2D), as expected for APs in pyramidal neurons of the motor cortex. We also compared ASAP5-Kv and ASAP3-Kv in the mouse hippocampus and found that ASAP5-Kv exhibited 80% higher SNR than ASAP3-Kv (Figures S2B and S2C). Finally, ASAP5-Kv was also superior to ASAP3-Kv in SNR in zebrafish tectal neurons under one-photon light-sheet microscopy (Figures S2D and S2E).

Interestingly, the higher single-AP SNR of ASAP5-Kv versus ASAP3-Kv and JEDI-2P-Kv derived from a larger relative fluo-

cence change ( $\Delta F/F_0$ ) without improved brightness. By contrast, the higher SNR versus JEDI-1P was due to only higher basal brightness ( $F_0$ ) (Figure 2C). That boosting either parameter can improve SNR is expected, as SNR in shot noise-limited conditions scales with  $\Delta F/\sqrt{F_0}$ , which equates to  $\Delta F/F_0 \times \sqrt{F_0}$  and thereby relates to both relative fluorescence change and basal brightness. Essentially, ASAP5 combines the larger  $\Delta F/F_0$  of JEDI-1P with the higher brightness of ASAP3 and JEDI-2P to improve one-photon SNR beyond earlier GEVs.

#### Single-trial imaging of graded potentials and APs in flies

We next compared ASAP5 and JEDI-2P responses in fruit flies under two-photon illumination. In *Drosophila*, Mi1 neurons depolarize when the fly is presented with a contrast increment on a gray background and hyperpolarize when contrast decrement is presented.<sup>17,18</sup> When expressed in Mi1, ASAP5 responses were approximately 100% larger in amplitude and 60% higher in SNR than JEDI-2P to both hyperpolarization and depolarization, while JEDI-2P displayed a 20% brighter baseline and slightly better photostability (Figure 3A). ASAP5 response amplitudes were also significantly larger than JEDI-2P when tested in L2 neurons, which hyperpolarize to contrast increment and depolarize to contrast decrement (Figure S3A).

Single-trial two-photon imaging of both graded responses and APs has not previously been reported in the fly. ASAP5 reported individual visually evoked excitatory and inhibitory graded potentials in Mi1; by comparison, visually evoked excitatory and inhibitory graded potentials were challenging to discern using JEDI-2P, given its lower SNR (Figure 3B). We also tested the ability of ASAP5 to detect APs in single trials, using the bilaterally symmetric pair of temperature projection neurons, TPN-II.<sup>19,20</sup> TPN-II neurons receive inputs from temperature receptor neurons and respond to changes in absolute temperature by modulating their spike rate. ASAP5 reported APs in TPN-II neurons using either resonant-galvanometric scanning at 779 fps or acousto-optic deflector (AOD)-based random-access scanning at 3.3 kHz, with similar SNR and multiple measurements per spike (Figures S3B and S3C). The ability of AODs to rapidly excite arbitrary locations allowed us to record both TPN-II neurons simultaneously at 3.3 kHz, and we found the two TPN-II neurons fired APs in an uncorrelated manner, consistent with receiving independent inputs (Figure 3C). Taken together, these experiments demonstrate that ASAP5 can detect both graded potentials and APs in single trials in the fly.

#### Single-trial imaging of APs and subthreshold potentials in mice

We next compared ASAP5-Kv and JEDI-2P-Kv in pyramidal neurons of the mouse cortex under two-photon illumination. Cell bodies of the neurons in the two groups were located at similar depths between 100 and 200 μm below the cortical surface (Figure 4A). ASAP5-Kv and JEDI-2P-Kv optical spikes recorded at

(C) Statistical analyses for  $\Delta F/F_0$  amplitude, cellular brightness averaged from the first second, SNR for detected optical spikes, and detected spike numbers (mean ± SEM). Outlined dots correspond with the displayed traces in (B). For  $\Delta F/F_0$  and SNR,  $p$  values are for one-way ANOVA with Bonferroni's multiple comparisons test. For brightness and detected spike numbers,  $p$  values are for Kruskal-Wallis test (non-parametric) with Dunn's multiple comparisons test. (D) An ASAP5-Kv expressing cortical neuron showing spikes time-locked to the running periods. The pseudo-colored bar below the fluorescence trace shows the running speed. Red ticks in (B) and (D) indicate spikes detected by VolPy.

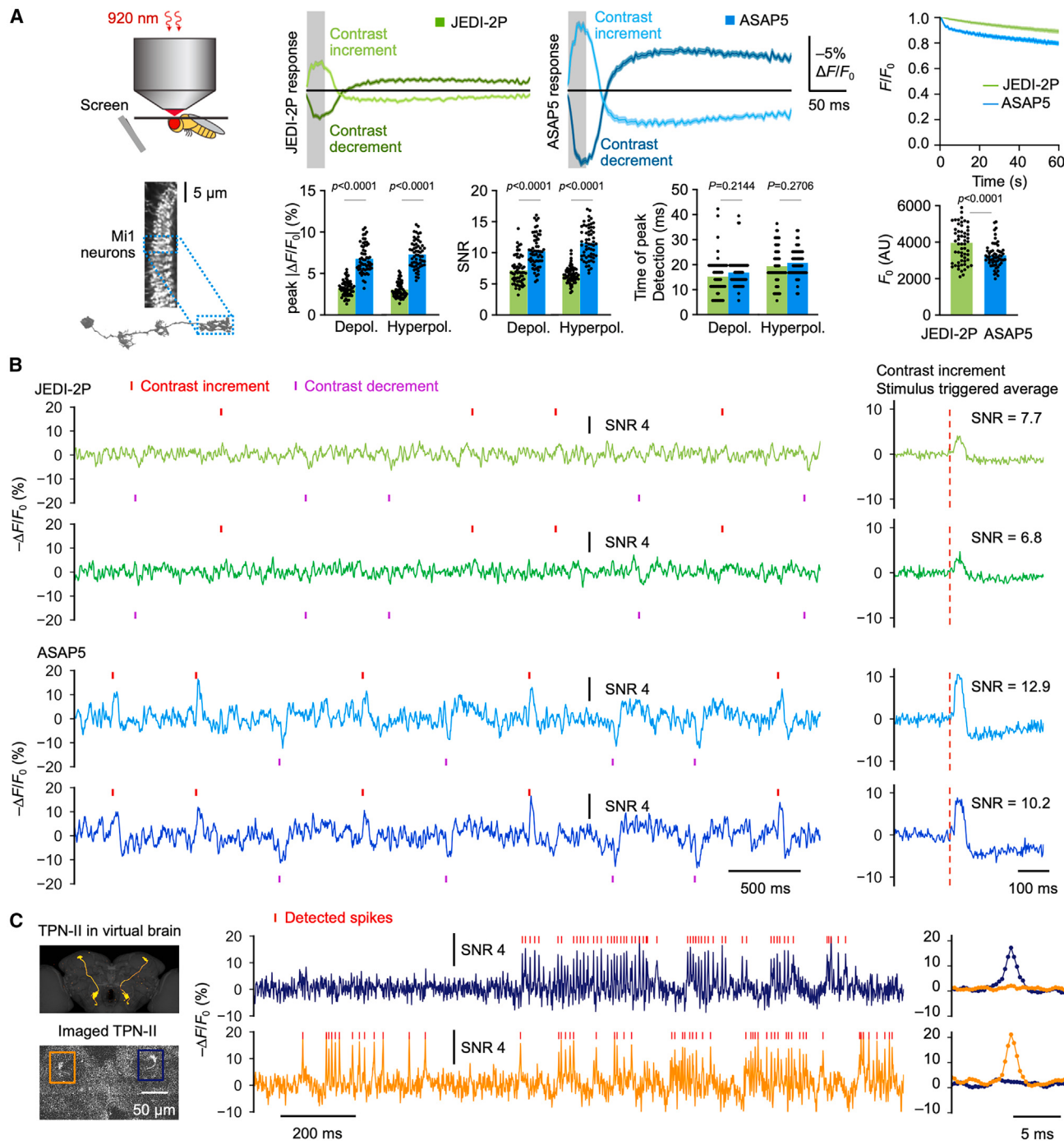


**Figure 3. Single-trial imaging of graded and action potentials in fruit flies**

(A) Comparison of ASAP5 and JEDI-2P in Mi1 neurons. Left: two-photon voltage imaging of Mi1 neurites in the M10 layer of the medulla in awake flies. Middle: stimulus-triggered average of fluorescence trace, peak response, SNR at peak, and time of detected peak response, in response to a 24-ms contrast increment or decrement (gray box). Right: photostability and baseline brightness of ASAP5 and JEDI-2P. Shadow represents SEM.  $n = 59$  ASAP5 neurons from 5 flies and 60 JEDI-2P neurons from 5 flies. Each dot represents one neuron. Welch's t test was used for all the comparisons and  $p$  values are reported.

(B) Left: example single trials of JEDI-2P or ASAP5-expressing Mi1 neurons responding to visual stimuli. Red ticks denote the onset of a 24 ms contrast increment; magenta ticks denote the onset of a 24 ms contrast decrement. Traces were binned to 70 fps. SNR scale was calculated on the whole trace. Right: stimulus-triggered average of the example traces. SNR value was calculated on the stimulus-triggered average.

(legend continued on next page)

500 fps were similar in response amplitude, but ASAP5-Kv exhibited higher brightness and higher SNR (Figure 4A). This differs from our observations with ASAP5 and JEDI-2P in fly Mi1 visual neurons, so we speculate that the relative brightness of the two indicators may depend on the presence of the soma-localization tag or on the experimental system. Remarkably, both ASAP5-Kv and JEDI-2P-Kv demonstrated exceptional photostability under two-photon illumination (Figure S4A). In one case, ASAP5-Kv reported voltage continuously at 500 fps for over 1 h without discernable reduction in SNR (Figure S4B). To obtain more precise measurements of optical spike width *in vivo*, we recorded single ASAP5-Kv-expressing pyramidal neurons in layer 2/3 of the mouse visual cortex at 7,142 fps by ultrafast local volume excitation (ULoVE) random-access two-photon microscopy (Figure S4D). The high sampling rate allowed partitioning of AP events into a slowly ramping summation phase and the rapid post-threshold spiking phase (Figure S4E). The full width at half maximum (FWHM) of the rapid optical spike varies from sub-millisecond to 2 ms (Figure S4E), demonstrating the fast kinetics of ASAP5.

Multi-unit voltage imaging is challenging with two-photon excitation because photons collected per voxel will drop with more locations or higher sampling rates. With higher labeling densities, raster scanning is economical,<sup>9,21</sup> whereas random-access strategies are better suited for more sparsely labeled specimens.<sup>14</sup> We expressed ASAP5-Kv sparsely in mouse motor cortex and recorded from multiple three-dimensional locations using a random-access two-photon microscope during locomotion. In one example, we recorded from 9 neuronal cell bodies distributed across  $-85$  to  $-278$   $\mu\text{m}$  in depth at 450 fps, observing contrasting relationships between locomotion and firing rates in individual neurons across long time scales (Figure S4C). These results demonstrate the feasibility of expanding random-access two-photon voltage imaging from two to three dimensions while increasing the number of recorded cells compared with previous work.<sup>10,14</sup>

Next, we used ASAP5-Kv to characterize the whisker selectivity of subthreshold excitatory and inhibitory responses by barrel cortex L2/3 pyramidal neurons. In anesthetized *in vivo* whole-cell recording experiments, whisker stimuli evoke excitation-inhibition sequences consisting of early EPSPs and spikes, followed by predominant inhibitory postsynaptic potentials (IPSPs) that suppress spiking.<sup>22–24</sup> To test whether somatotopically tuned EPSPs, spikes, and IPSPs can be detected *in vivo*, we imaged ASAP5-Kv-expressing cells in the awake mouse barrel cortex while stimulating 9 whiskers in randomized order, using a standard resonant-galvanometric two-photon microscope (Figure 4B). For cells imaged in the C2 column, the C2 whisker evoked strong EPSP amplitude and spike frequency, while the D2 whisker did not (Figure 4C). The early EPSP and spikes were followed by a later optical hyperpolarization, indicating an IPSP. For individual cells, whisker-evoked optical EPSP and IPSP magnitude were correlated, consistent with predicted

fine-scale balance between excitation and inhibition in sensory computations<sup>25</sup> (Figure 4D). Across multiple imaging fields, clear somatotopic tuning for EPSPs, IPSPs, and spikes was observed (Figure 4E). These results extend earlier demonstrations of sub-threshold EPSP detection by ASAP-family indicators<sup>21</sup> to IPSPs and show that ASAP5 can be used to study the tuning and timing relationships between EPSPs and IPSPs. Interestingly, these findings could not have been made by calcium indicators, which lack the ability to detect inhibitory inputs.

#### Optical detection of mEPSPs in cultured rat neurons

Spontaneous exocytosis of single synaptic vesicles continues when APs are blocked by tetrodotoxin (TTX) to produce mEPSPs, whose frequency and amplitude reflect synaptic number and function.<sup>26</sup> To determine if ASAP5-Kv can detect mEPSPs at the soma, we performed simultaneous fluorescence imaging and whole-cell electrophysiological recording of cultured neurons in the presence of TTX and picrotoxin (PTX) to remove APs and inhibitory potentials (Figure 5A) and identified mEPSPs in both traces by a deconvolution-based algorithm<sup>27</sup> (Figures S5A–S5C). As a comparison, we also imaged Voltron2-Kv labeled with the JaneliaFluor525 fluorophore (Voltron2<sub>525</sub>-Kv), the combination of protein and chemical dye with the largest response per mV in the Voltron chemogenetic voltage indicator system<sup>15</sup> (Figure 5B). As the excitation and emission spectra of ASAP5 and JaneliaFluor525 are different, we calculated the relative efficiency of ASAP5-Kv in fluorescence excitation and collection compared with Voltron2<sub>525</sub>-Kv given the filter sets we used, then added shot noise to the ASAP5-Kv trace to compensate for its better excitation and collection so that SNR would mimic the situation where ASAP5-Kv had similar excitation and collection efficiency to Voltron2<sub>525</sub>-Kv. Although brightness per cell of Voltron2<sub>525</sub>-Kv was 4.1-fold higher than that of ASAP5-Kv (after adjusting for filter efficiency, Figure S5D), SNRs for mEPSPs were similar (Figure 5C). The ability of ASAP5-Kv to match Voltron2<sub>525</sub>-Kv in SNR was due to its larger responsivity of  $-0.83\%/\text{mV}$  compared with  $-0.48\%/\text{mV}$  (Figure 5C) and the fact that SNR scales linearly with response size but only with the square root of brightness.<sup>28</sup> Optical waveforms of detected mEPSPs were similar in shape between ASAP5-Kv and Voltron2<sub>525</sub>-Kv (Figure 5D), and cross-correlograms between optical and electrophysiological recordings were also similar (Figure 5D), implying no substantial differences in kinetics between the two systems. At excitation rates that produce similar SNR, ASAP5-Kv and Voltron2<sub>525</sub>-Kv exhibited similar photostability (Figure S5E).

Next, we quantified and compared the false positive (FP) rate, defined by the proportion of optically detected events without a corresponding mEPSP in the voltage trace, and false negative (FN) rate, defined by the proportion of electrically detected events without a corresponding mEPSP event in the optical trace. The two systems exhibited similar FP and FN rates across the 0–3 mV range of mEPSP amplitudes (Figure 5E). For mEPSPs

(C) Left: the scanned image of the fly brain with two ASAP5-expressing TPN-II neurons and a template fly brain showing R60H12-Gal4 expression pattern. Middle: example traces of two ASAP5-expressing TPN-II neurons firing spikes recorded using a 3D AOD random-access scope (FemtoNics) at 3,288 fps. Gaussian filter ( $\sigma = 1.5$  frame) was applied to the trace. Red ticks denote the peaks of each spike. Right: averaged waveform of all spikes in each cell, as well as the spike-triggered average of the response of the other neuron. Dots represent the measurement points.

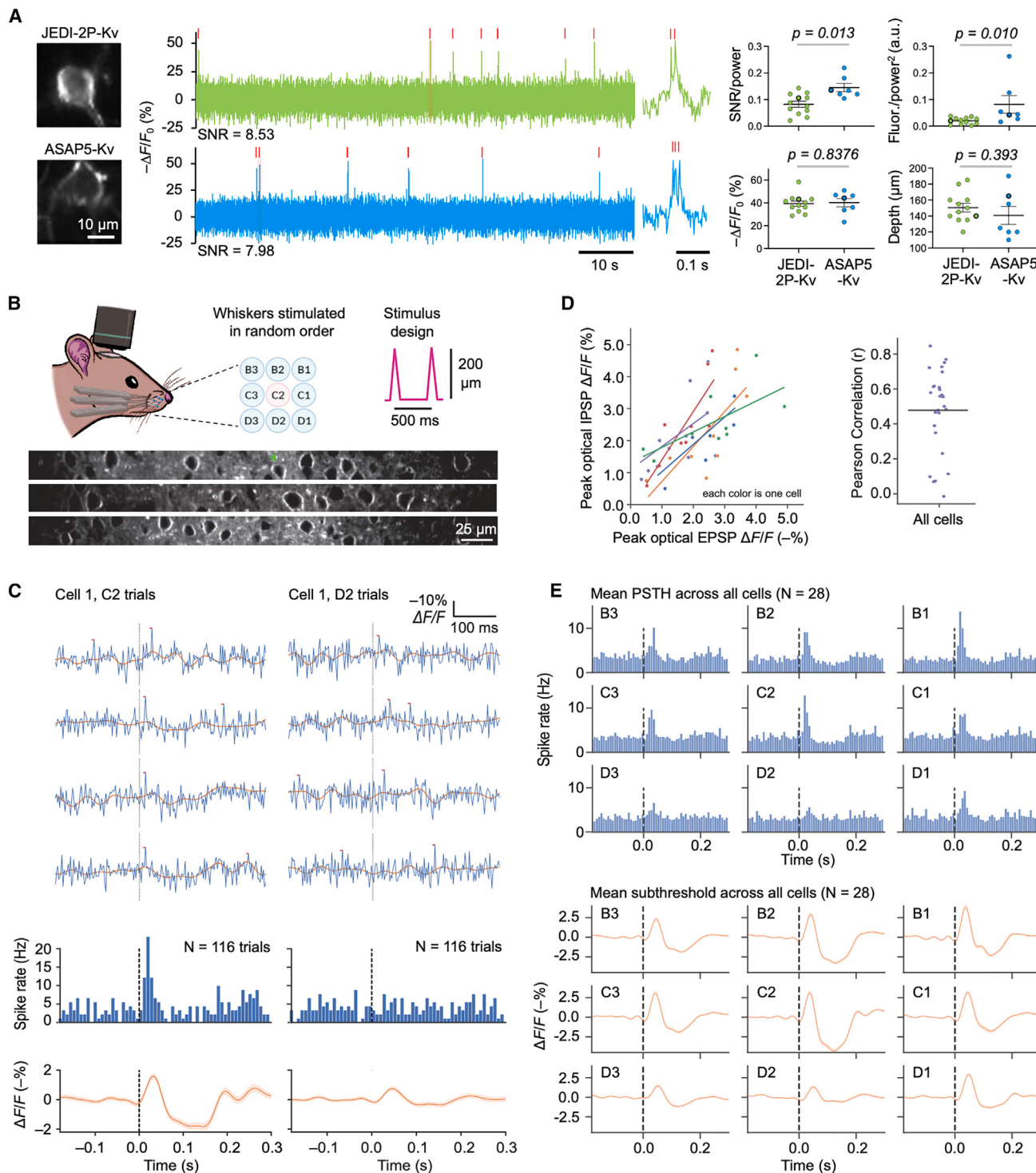


**Figure 4.** Single-trial two-photon imaging of supra- and subthreshold activities in awake mice

(A) Comparison of ASAP5-Kv and JEDI-2P-Kv two-photon performance. Left: representative layer 2 motor cortex neurons expressing JEDI-2P-Kv or ASAP5-Kv. Middle: corresponding baseline-corrected fluorescence traces, with shaded intervals enlarged at the right. Right: comparison of SNR and brightness corrected for post-objective power (mW) used for each neuron, spike amplitudes in  $\Delta F/F_0$ , and depth of each neuron from dura (mean  $\pm$  SEM).  $n = 12$  JEDI-2P-Kv cells from 3 mice and 7 ASAP5-Kv cells from 4 mice. Outlined dots correspond with the displayed traces. For SNR and brightness,  $p$  values are for Mann-Whitney tests. For spike amplitudes and depth,  $p$  values are for unpaired t tests.

(legend continued on next page)

with amplitudes >1 mV, both sensors reported mEPSPs with an FP rate of <20%. To cross-validate the comparison results, we also used the machine-learning algorithm miniML<sup>29</sup> to detect optical mEPSPs after training on paired segments of electrical and optical recordings, or after training on electrical recordings only. In these analyses, ASAP5-Kv and Voltron2<sub>525</sub>-Kv again produced similar FP and FN rates (Figures 5F and S5F).

Taken together, these results demonstrate that both ASAP5-Kv and Voltron2<sub>525</sub>-Kv can be used in cultured neurons to detect spontaneous synaptic events at the cell body in the single-mV range using standard illumination conditions (~46 mW/mm<sup>2</sup>). Between these systems, ASAP5-Kv has the advantage of being completely genetically encoded without requiring the addition of a chemical dye.

### Recording propagations of synaptic inputs along dendrites

Constructing accurate models of neuronal computation requires understanding how synapses in dendritic trees signal to the site of AP generation in the cell body. Voltage signals originating at synapses attenuate as they propagate passively along dendrites, with the distance of the synaptic input to the soma influencing the degree of attenuation.<sup>30–32</sup> Previous studies have demonstrated the imaging of EPSPs in the dendritic spines *in vitro* using ASAP1<sup>33</sup> or *in vivo* using postASAP.<sup>12</sup> However, single-trial visualization of EPSP propagation from dendrites to soma has not yet been demonstrated. We therefore imaged pan-membrane ASAP5 in cultured neurons (Figure 6A). We observed low-amplitude ASAP5 transients in the cell body that correlated with low-amplitude EPSPs recorded by simultaneous whole-cell electrophysiology and were clearly distinct from APs (region of interest [ROI] 1). These somatic ASAP5 signals correlated with larger fluorescence transients in one primary dendrite but not another primary dendrite (ROI 4 or 7), further confirming they are not back-propagating APs. Centripetal decay of these transients was apparent along the dendrite toward the cell body.

Next, we investigated the relationship between initial locations of mEPSPs and their initial and final amplitudes, imaging pan-membrane ASAP5 in cortical neurons with TTX and PTX. For each mEPSP, we defined the location with the highest signal amplitude as the initiation site of the event and measured the corresponding somatic signal (Figure 6B). We first asked how the amplitude of the same mEPSP event at the initiation point ( $V_D$ ) or at the soma ( $V_S$ ) correlates with the distance between the two locations ( $d_{DS}$ ). We found that  $V_D$  positively correlated with  $d_{DS}$  in individual examples (Figure 6C) and across most neurons (Figure 6D), while  $V_S$  negatively correlated with  $d_{DS}$

(Figures 6C and 6D). As a result, the attenuation coefficient  $A_{DS} = V_D/V_S$  positively correlated with  $d_{DS}$  (Figures 6C and 6D). Overall, these results suggest that a greater distance between the dendritic input site and the soma correlates with a larger initial voltage signal, a smaller somatic voltage signal, and higher attenuation during the propagation. These observations are consistent with previous electrophysiological measurements in brain slices.<sup>32,34</sup>

Cable theory predicts exponential decay of mEPSP amplitude as signals propagate passively along the dendrite.<sup>35</sup> At the same time, precise quantification of spatial attenuation and determination of the length constant is challenging using electrophysiological approaches in many neurons, as these measurements require multiple patch recordings at different locations along the same dendrite. We therefore asked if we could directly measure voltage changes along multiple points of each dendrite to map spatial attenuation using voltage imaging. For each propagation event, we correlated the distance between the peak ASAP5 signal at each point along the dendrite and the soma and fit it with an exponential function (Figure 6B) to estimate the length constant. The measured length constants varied from 25 to 240  $\mu\text{m}$ , with an average of 90  $\mu\text{m}$  (Figure 6E). These signals were inhibited by 6-cyano-7-nitroquinoxaline-2,3-dione (CNQX), identifying them as mediated by GluA receptors (Figure S6A).

In addition, we observed network effects in cultured rat cortical neurons without channel blockers, with either pan-membrane ASAP5 or soma-localized ASAP5-Kv (Figures S6B and S6C), with neuron pairs displaying shared activating inputs. IPSP-like events could also be detected (Figure S6B). Taken together, these results suggest that ASAP5 can be used to study the passive and active propagation of EPSPs and the effects of IPSPs. These excitatory and inhibitory PSPs and synchronized spiking activities from two neurons are examples of mixed sub- and suprathreshold network-dependent activity that would be difficult to observe by multi-electrode arrays (MEAs) or calcium imaging.

### Reporting network activity and unitary synaptic events in human neurons

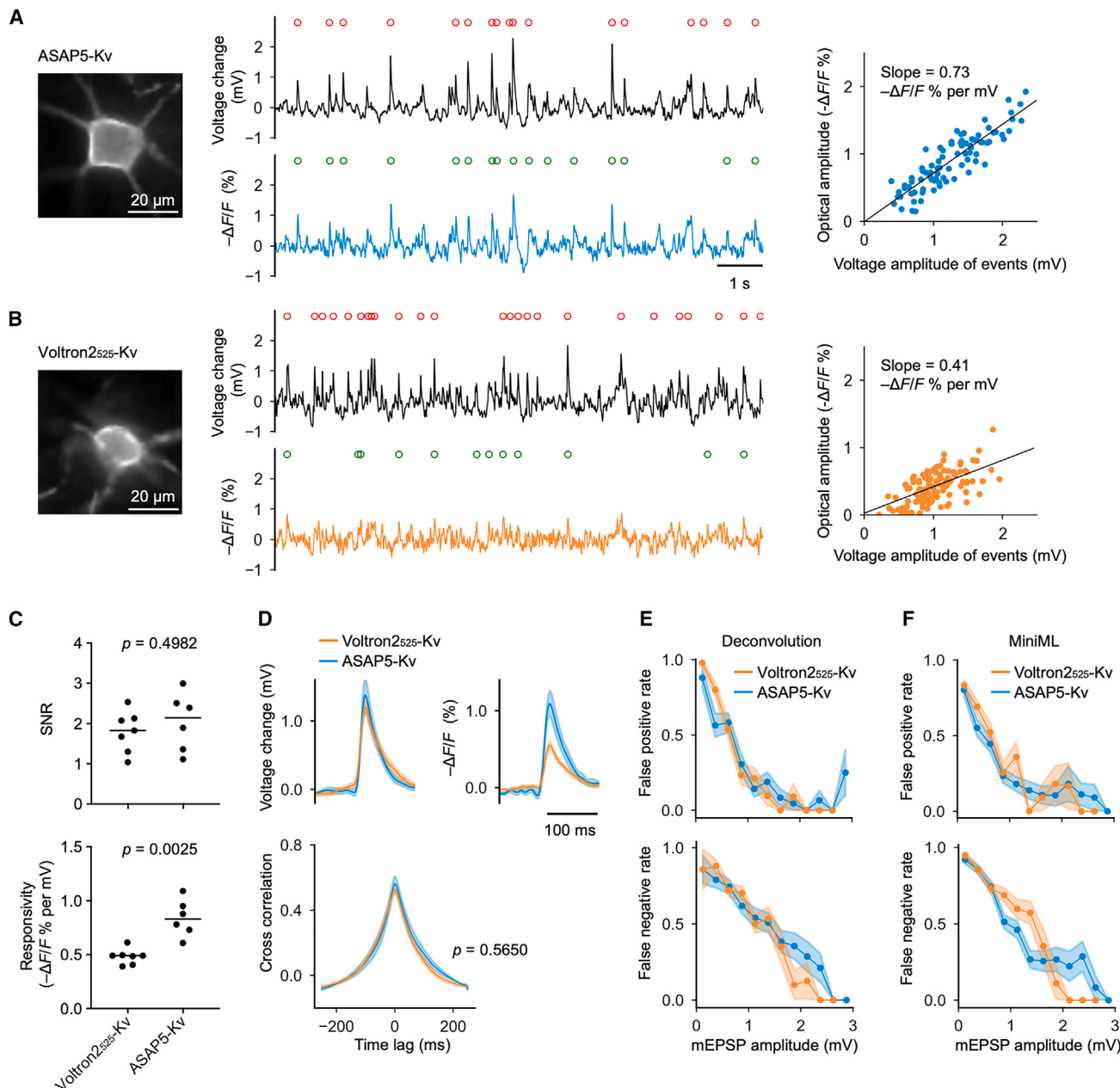
Patch-clamp electrophysiology, MEAs, and calcium imaging have been widely used to study the effects of disease-associated mutations in human stem-cell-derived neuronal cultures. Patch-clamp electrophysiology remains the gold standard in its ability to detect both spiking and subthreshold activity, but can only be performed on a handful of neurons at a time. As large sample sizes are required to detect small differences in mEPSP

(B) Schematic of voltage imaging in mouse barrel cortex during whisker stimulation and representative images of ASAP5-Kv in layer 2 neurons. Green arrowhead, a neuron in the C2 column analyzed in (C).

(C) Top: ASAP5-Kv traces from a neuron responding to stimulation on either C2 or D2 whisker, imaged at 397 fps. The orange line is the subthreshold component obtained by a long-pass filter. Middle: post-stimulus time histogram (PSTH) showing spike rates during whisker stimulation. Bottom: averaged subthreshold traces for C2 (left) or D2 (right) whisker stimulation.

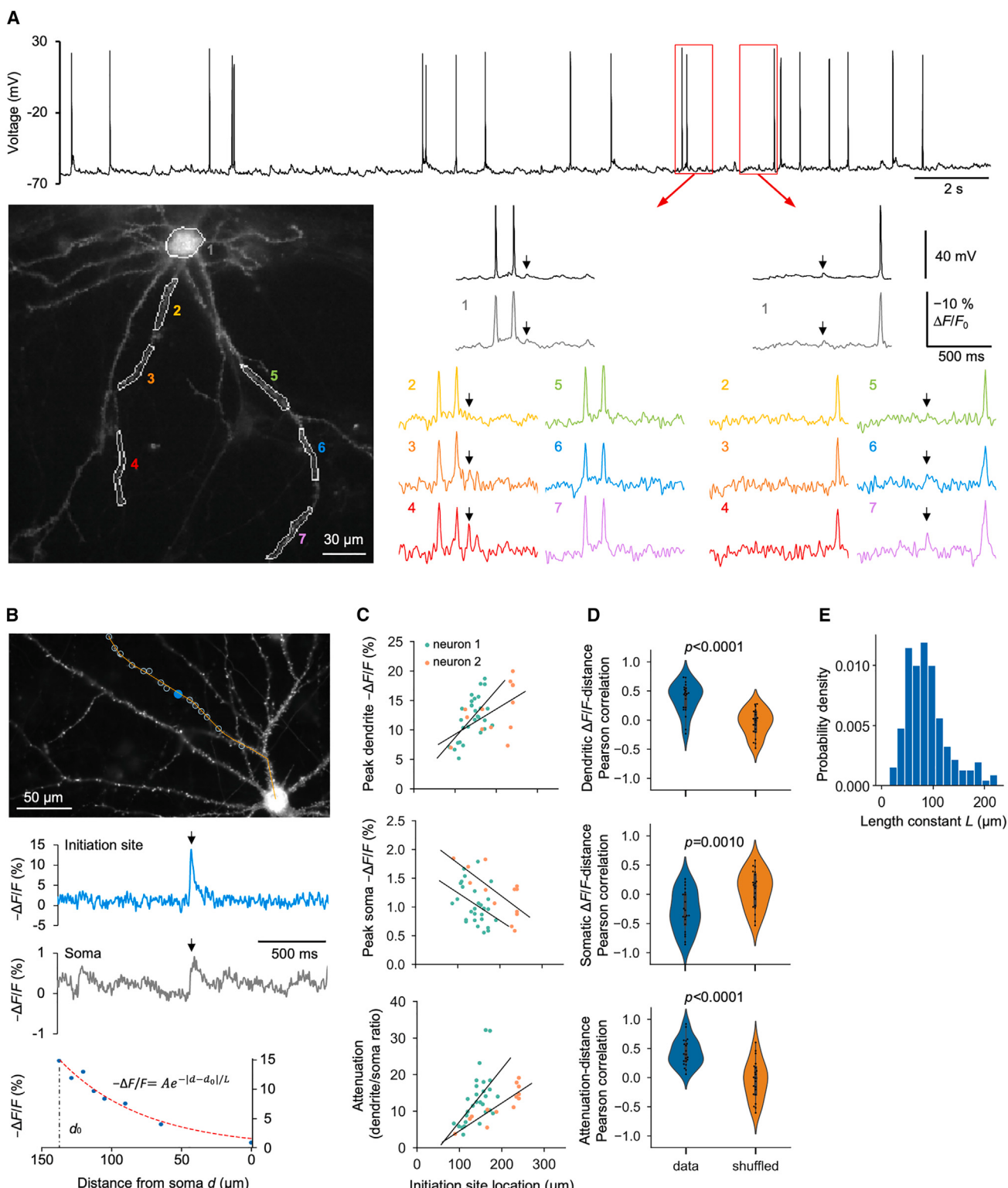
(D) Correlation between whisker-evoked EPSP and whisker-evoked IPSP amplitude for 5 cells imaged in the same field (colors). Lines show linear regression for each cell. Right: distribution of Pearson's correlation coefficient for each cell ( $n = 28$ ), showing that whisker-evoked excitation and inhibition are generally correlated. Neurons were in the C2, B1, or C1 columns.

(E) Top: mean PSTH of all cells ( $n = 28$ ) for each stimulated whisker. Bottom: mean fluorescence traces across all cells ( $n = 28$ ) showing subthreshold activity for each whisker stimulation. Dashed lines in (C) and (E) represent stimulus onset.



**Figure 5. Optical detection of mEPSPs in cultured rat hippocampal neurons**

- (A) Left: a neuron expressing ASAP5-Kv. Middle: simultaneous voltage and optical recording of the neuron. The voltage recording was downsampled to match the optical recording. Red circles denote mEPSPs detected in the voltage recording. Green circles denote mEPSPs detected in the optical recording. Right: the amplitude of mEPSP voltage signals and the corresponding optical signals from the example neuron. Black line is the linear fitting of the data.
- (B) A neuron expressing Voltron2<sub>525</sub>-Kv and the recording of mEPSPs. Panels are the same with (A).
- (C) Top: SNR of the peak amplitude of mEPSPs. Bottom: responsivity of the indicators for reporting mEPSPs. Each dot is a neuron. Welch's t test was used for statistical comparison of the mean.
- (D) Top, mean electrical waveforms (left) and optical waveforms (right) of detected mEPSPs of the two sensors. Each optical waveform was normalized to its peak value for comparing kinetics. Bottom: time-lagged cross-correlograms of simultaneous voltage and optical recordings. Shaded area: SEM. Number of neurons: 6 (ASAP5-Kv) and 7 (Voltron2<sub>525</sub>-Kv). Welch's t test was used to compare the mean of the peak cross-correlations.
- (E) Fidelity of optical detection of mEPSPs using deconvolution-based method. Top: averaged false positive (FP) rate as a function of mEPSP amplitude for all events from all neurons. Bottom: averaged false negative (FN) rate as a function of mEPSP amplitude for all events from all neurons. Shaded area: SEM. Number of neurons and events detected per neuron: 6, 89 ± 31 (ASAP5-Kv; mean ± SD) and 7, 61 ± 29 (Voltron2<sub>525</sub>-Kv; mean ± SD).
- (F) Fidelity of optical detection of mEPSPs using miniML trained on paired electrophysiological and optical recordings. Top: averaged FP rate as a function of mEPSP amplitude for all events from all neurons. Bottom: averaged FN rate as a function of mEPSP amplitude for all events from all neurons. Shaded area: SEM. Number of neurons and events detected per neuron: 6, 144 ± 97 (ASAP5-Kv; mean ± SD) and 7, 97 ± 99 (Voltron2<sub>525</sub>-Kv; mean ± SD).

**Figure 6. Voltage imaging of dendrosomatic propagation of mEPSPs**

(A) ASAP5 reveals EPSPs originating from distal dendrites in a rat hippocampal neuron (DIV 26). Top: whole-cell current-clamp recording of spontaneous activity. The red boxes indicate two time periods shown below. Bottom left: a time period where the dendritic ROIs 2, 3, and 4 (from proximal to distal) show subthreshold events with decreasing  $\Delta F/F_0$  amplitudes as it propagates from distal to the soma (marked by a black arrow). Note that these dendritic EPSPs are not present in

(legend continued on next page)

frequency due to the intrinsic variability in mEPSP rate between neurons, the limited throughput of patch-clamp electrophysiology limits assessment of synaptic function in neuronal populations using this approach. By contrast, MEAs and calcium imaging allow parallel detection of spiking activity in multiple neurons, allowing assessment of changes in overall network excitability by mutations found in neurological disease such as autism and schizophrenia.<sup>36</sup> However, neither MEAs nor calcium can directly detect subthreshold or inhibitory activity, and MEAs do not allow genetic specification of recorded cell types.

Previously, an opsin-based GEVI, a two-component chemogenic voltage indicator, and a small-molecule voltage-sensitive dye have been used to measure neuronal excitability of human stem-cell-derived neurons by AP detection.<sup>37–39</sup> We asked if ASAP5 could extend the uses of voltage imaging in human neurons to EPSP detection. We differentiated human embryonic stem (ES) cells into neurons using an established protocol,<sup>40</sup> introduced ASAP5-Kv by lentiviral transduction, and performed one-photon imaging at 400 fps. In one example, activity between two human-induced neurons (human iNs) was correlated in multiple ways (Figure 7A; Video S2): EPSPs in both neurons, an AP in one neuron with a corresponding EPSP in the other, or APs in both neurons (Figure 7A, bottom). Because simulations demonstrated that 100 fps was as effective as faster imaging frame rates in detecting subthreshold activity, while preserving distinctly sharper optical responses to APs (Figure S7A), we imaged human iNs at this lower speed to acquire a larger field of view (FOV). This allowed the observation of correlated APs and EPSPs in up to 8 human iNs simultaneously (Figure 7B).

We hypothesized that ASAP5-Kv could also be used to detect mEPSPs in human iNs. Abnormalities in synapse development or vesicular release probability caused by disease-associated mutations are manifested as altered mEPSP or mEPSC frequencies, but phenotypes can differ between human iNs and rodent neurons, underscoring the importance of studying human iNs.<sup>41</sup> As most synaptic activity studies in human iNs used somatic voltage-clamp recordings to detect mEPSCs rather than mEPSPs, we first compared somatic current-clamp and voltage-clamp recordings with TTX and PTX to allow only spontaneous quantal glutamate release.

Both mEPSCs and mEPSPs were detected with similar frequency (Figure S7B) and did not occur in the presence of the GluA channel blocker CNQX, indicating that these were excitatory synaptic events.<sup>40</sup> Finally, to assess our ability to image mEPSPs, we conducted simultaneous current-clamp recording and ASAP5-Kv imaging in human iNs in the presence of TTX and PTX. ASAP5-Kv detected mEPSPs with amplitudes as low as 1 mV, with a mean  $\Delta F/F_0$  of  $-0.67\%$  per mV depolarization for the example neuron (Figure 7C). These results demonstrate that mEPSPs, representing synaptic quantal events, can be easily detected in cultured human iNs.

## DISCUSSION

ASAP5 is an improved GEVI with 0.78 ms onset kinetics at physiological temperature, larger responses to APs and subthreshold events, achieving single-trial EPSP and IPSP detection at cell bodies *in vivo* and 1-mV responsivity in cultured neurons. ASAP5 exhibits higher sensitivity and SNR than JEDI-2P and JEDI-1P for detecting spikes *in vivo* while achieving similar SNR to Voltron2 for detecting mEPSPs in cultured neurons. With its superior SNR for both sub- and suprathreshold activities, ASAP5 enabled single-trial two-photon recordings of graded potentials and APs in fly neurons, of APs at multiple 3D locations in motor cortex, and of EPSP and IPSPs in barrel cortex. Most importantly, with its higher gain near resting membrane potentials, ASAP5 enabled optical recording of unitary synaptic events in human neurons, previously only achievable with patch-clamp electrophysiology. ASAP5 detected coordinated APs and EPSPs in multiple human neurons within a network, a feat not possible with MEAs and challenging for conventional patch clamping.

ASAP5 conveniently maintains large responses across imaging modalities. Under one-photon excitation of sparsely labeled neurons *in vivo*, ASAP5 showed higher SNR than previous ASAP-family GEVIs. When used in cultured neurons, where the specimen is nearly two dimensional, out-of-focus cells are not a problem, and thus, ASAP5 provides excellent sensitivity even from very densely labeled specimens. So far, one-photon imaging of soma-targeted GEVIs has been demonstrated through

---

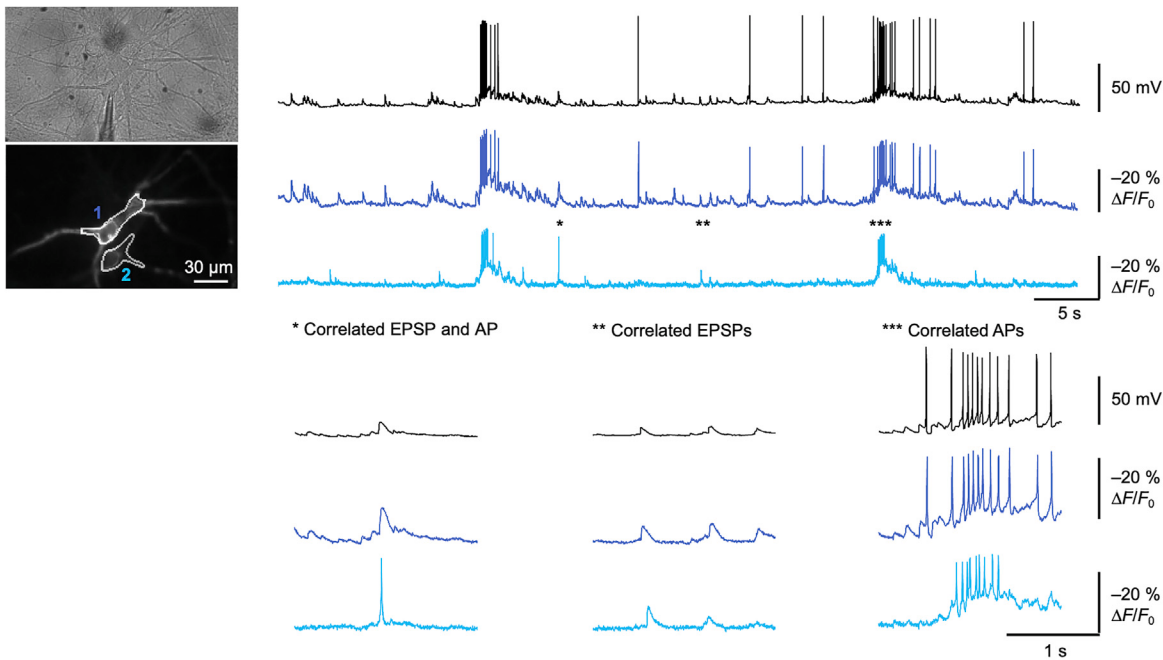
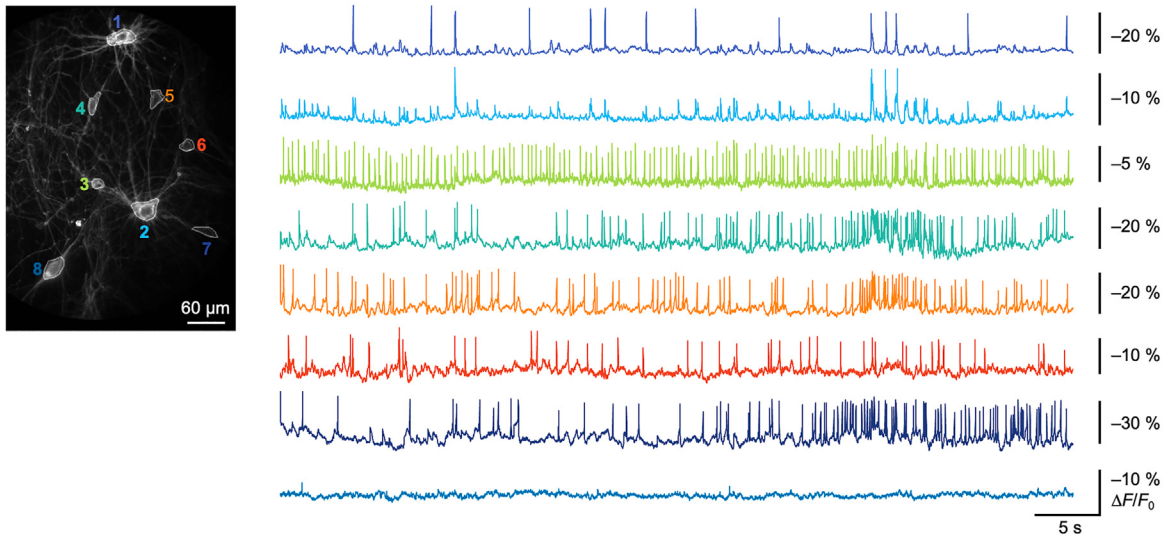
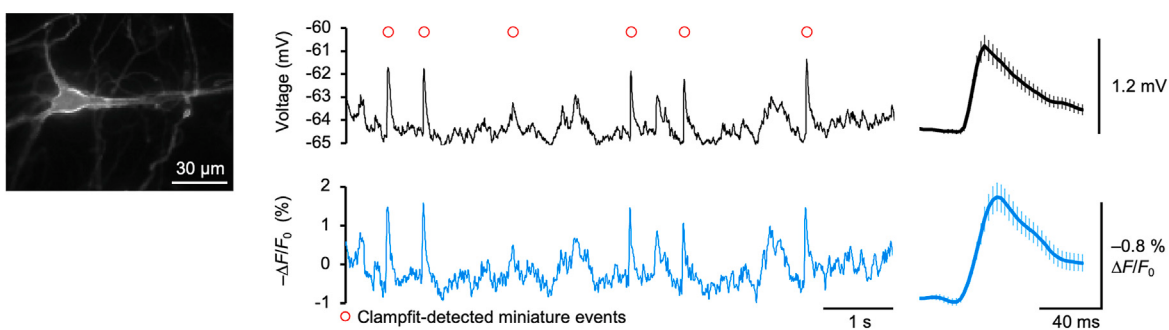
ROIs 5, 6, and 7, which are on another dendrite. Bottom right: another time period where ROIs 5, 6, and 7, but not ROIs 2, 3, and 4, are showing a dendritic EPSP with larger amplitudes in distal part than in near-soma ROIs.

(B) An example neuron and an observation of the spatial propagation of mEPSP. Top: an example neuron expressing ASAP5. The blue solid disk marked the initiation site of the propagation, and the blue circles marked the pixels with coincident optical signals. The yellow line marked the path along which the distance to soma was calculated. Middle: the optical traces of the propagation event at the initiation site and the soma. Black arrows indicate the time of the peak signals of the propagation. Bottom: the amplitudes of the optical signals in the propagation event as a function of the distances between the pixels and the soma.  $d_0$  marked the distance of the initiation site to the soma. Only the signals from pixels closer to the soma than the initiation site were included. The red dashed line is the exponential function that fits the data.

(C) Top: amplitude of signals at the initiation sites correlates with the distance between the initiation site and the soma. Middle: amplitude of signals at the soma correlates with the distance between the initiation site and the soma. Bottom: dendrosomatic attenuation ratio correlates with the distance between the initiation site and the soma. In the three plots, each dot is a propagation event, and each color is a neuron. Two example neurons are shown here, and the black lines are the linear fit of the data.

(D) Top: the Pearson correlation coefficients of signal amplitude at the initiation sites and the distance between initiation site and soma. Middle: the Pearson correlation coefficients of signal amplitude at the soma and the distance between initiation site and soma. Bottom: the Pearson correlation coefficients of dendrosomatic attenuation ratio and the distance between the initiation site and the soma. In the three plots, each dot is a neuron. Number of neurons: 21.  $p$  values are for the Welch's t tests. Shuffled control is the Pearson correlations of the two paired variables but with shuffled pairing.

(E) Histogram of the length constant  $L$  fit from the exponential function in (B) for all propagation events from all neurons. Number of neurons and propagation events: 21, 309.

**A****B****C**

(legend on next page)

300  $\mu\text{m}$  of tissue using a combination of targeted illumination and confocal gating,<sup>42</sup> while two-photon voltage imaging with sub-cellular resolution has been performed through 600  $\mu\text{m}$  of tissue.<sup>10</sup> Two-photon excitation is therefore still essential when imaging deeper below the surface and useful for reducing background in densely labeled specimens as out-of-focus cells are not excited. Under two-photon excitation by resonant-galvanometric scanning or random-access scanning, ASAP5 was superior in SNR to previous GEVLs. While we did not re-test opsin-based indicators under two-photon scanning, these are now well known to show greatly diminished and pattern-dependent responses with two-photon scanning,<sup>43,44</sup> which may derive from the kinetics of their multi-state photocycles.<sup>45,46</sup> Thus, ASAP5 is widely useful *in vivo* under one-photon excitation with sparse labeling, *in vivo* under two-photon excitation at any labeling density, or *in vitro* under any illumination.

We note that one characteristic of ASAP5 is that it, like ASAP3, is not compatible with two-photon excitation at wavelengths beyond 1,020 nm. By contrast, the fluorophores of JEDI-2P and ASAP4 exhibit slightly red-shifted excitation spectra due to the presence of a  $\pi$ - $\pi$  stacking interaction between a histidine residue and the chromophore.<sup>47</sup> JEDI-2P and ASAP4 can be excited on their right shoulder by 1,030-nm ytterbium-doped fiber lasers with high output powers.

The high responsivity of ASAP5 near the resting membrane potential, which enhances the detection of mEPSPs at soma and along the dendrites *in vitro*, should also aid the detection of EPSPs and their spatial propagation *in vivo*. Recently, an ASAP-family sensor has been targeted to synapses for imaging dendritic spines *in vivo*.<sup>12</sup> Substitution of ASAP5 may allow higher SNR recording of dendritic spines and shafts for studying dendritic integration. In addition, given our ability to detect APs in 9 cell bodies *in vivo* by random-access multiphoton microscopy, it should be feasible to apply the same method to record voltage at multiple dendritic locations at 500–1,000 fps. This should open opportunities for studying how neurons integrate responses to naturalistic stimuli and how integration is altered by neuromodulation or by learning.

With its enhanced SNR for electrical events from 1 to 100 mV, ASAP5 should enable high-throughput characterization of synaptic and network function in stem-cell-derived human neurons in culture. Specifically, ASAP5 can report all levels of electrical activity—APs, EPSPs and IPSPs, and mEPSPs—in multiple neurons in parallel. ASAP5 should thus allow high-throughput functional characterization of physiological phenotypes of mutations associated with neuropsychiatric diseases such as autism, schizophrenia, and neurodegenerative disorders, substituting

for low-throughput patch-clamp electrophysiology for many tasks. Finally, the improved throughput of voltage imaging may open up possibilities for directly screening drug libraries for improved synaptic function in human neurons.

#### RESOURCE AVAILABILITY

##### Lead contact

Further information and requests for resources and reagents should be directed to and will be fulfilled by the lead contact, Michael Z. Lin ([mzlin@stanford.edu](mailto:mzlin@stanford.edu)).

##### Materials availability

Plasmids generated in this study have been deposited to Addgene.

1. pAAV-hSyn-ASAP5-Kv, ID: 225707
2. pAAV-hSyn-ASAP5, ID: 225709
3. pAAV-EF1a-Dio-ASAP5-Kv, ID: 225708

Transgenic flies generated in this study have been deposited to Bloomington Drosophila Stock Center.

1. w[+]; P{20XUAS-ASAP5}attP40/CyO; TM2/TM6B. ID: 605336
2. w[+]; S[1]/CyO; PBac{20XUAS-ASAP5}VK00005/TM6B. ID: 605337
3. P{20XUAS-ASAP5}attP40/CyO; PBac{20XUAS-IVS-NES-jRGECO1a-p10}VK00005/TM6B. ID: 605338

##### Data and code availability

- All data reported in this paper will be shared by the [lead contact](#) upon request.
- All original code has been deposited at Zenodo and is publicly available as of the date of publication (Zenodo: <https://doi.org/10.5281/zenodo.13760547>).
- Any additional information required to reanalyze the data reported in this paper is available from the [lead contact](#) upon request.

#### ACKNOWLEDGMENTS

We thank the Stanford Gene Vector and Virus Core for viral vector packaging; Lan Xiang Liu (Stanford University) for animal care; Fuu-Jiun Hwang and Yue Sun (Stanford University) for advice and help on virus injection and brain tissue preparation; Femtonics for the loan of the 3D AOD two-photon microscope; Christian Thome, Kristin Arendt, and Lu Chen (Stanford University) and Min-Ho Nam (Korea Institute of Science and Technology) for advice on electrophysiological recording of mEPSPs and event detection; Richard W. Tsien for advice on voltage imaging of dendritic propagation; and the late Lawrence B. Cohen for inspiring us to improve voltage indicators. This work was funded by NIH grants R01NS12368101 (T.R.C., J.D., P.G., N.J., and M.Z.L.), R01NS116589 (M.Z.L., P.G., and J.T.), R01EY022638 (T.R.C.), UF1NS107696 (N.J. and L.G.), U01NS118300 (N.J. and L.G.), R01MH123977 (E.B. and Z.W.), and R01DA029639 (E.B. and Z.W.). E.B. was also funded by MIT Alana Center, Lisa Yang, and HHMI. Y.A.H. was funded by the Stanford Bio-X Bowes Fellowship.

#### Figure 7. Characterization of electrical activity in induced human neurons by ASAP5-Kv

- (A) Two human iNs expressing ASAP5-Kv under the ubiquitin-C (UbC) promoter imaged at 40 DIV. Cell 1 was patched in whole-cell mode for simultaneous recording of its spontaneous activity in electrophysiology (black) and in ASAP5-Kv fluorescence (dark blue). Cell 2 was only imaged for its fluorescence change (blue). The asterisks indicate three exemplary states of the two cells, and their zoomed-in traces are shown on the lower panel. Frame rate was 400 fps.
- (B) Eight ASAP5-Kv expressing human iNs network (hSyn promoter; 41 DIV) imaged at 100 fps revealing their supra- and subthreshold activity in cellular resolution.
- (C) Left: a human iN expressing virally introduced ASAP5-Kv (hSyn promoter; 80 DIV). Middle: simultaneous recording of spontaneous activity in electrophysiology (black) and ASAP5-Kv fluorescence (blue) with TTX (1  $\mu\text{M}$ ) and PTX (50  $\mu\text{M}$ ) in the bath solution to block AP-generated synaptic activity and inhibitory transmission. The red circles indicate miniature events detected by using a template search algorithm. Right: averages of electrical (black) and fluorescent signal (blue) for 42 mEPSPs recorded from the same neuron during 1 min. Error bars: SEM.

**AUTHOR CONTRIBUTIONS**

Y.A.H. engineered and characterized ASAP5, performed the fly experiments, analyzed data, prepared figures, and co-wrote the manuscript. S.L. performed experiments in cultured neurons and human ES-derived neurons, performed one-photon benchmarking in mouse motor cortex experiments, analyzed data, prepared figures, and co-wrote the manuscript. R.H.R. performed mouse motor cortex experiments and analyzed data. S.N. generated human ES-derived neurons. L.G. performed mouse barrel cortex experiments, analyzed data, and prepared figures. M.S. and D.L. tested viral constructs in the mouse. J.T. performed mouse hippocampus experiments. P.S.O. performed miniML detection of miniature synaptic events from cultured neurons and analyzed data. V.V. and J.B. performed mouse visual cortex experiments and analyzed data. Z.W. performed zebrafish experiments. D.J. performed initial mEPSP analyses. G.Z. characterized ASAP5 intermediates. E.B., I.D., P.G., M.W., D.E.F., N.J., J.D., T.C.S., and T.R.C. provided supervision, advised on experimental design, and assisted with data interpretation. M.Z.L. conceived of the project, provided supervision, advised on experimental design, assisted with data interpretation, prepared figures, and co-wrote the manuscript.

**DECLARATION OF INTERESTS**

M.Z.L. is an inventor on a patent for the earlier ASAP1 voltage indicator.

**STAR METHODS**

Detailed methods are provided in the online version of this paper and include the following:

- **KEY RESOURCES TABLE**
- **EXPERIMENTAL MODEL AND STUDY PARTICIPANT DETAILS**
  - Cultured cell lines
  - Primary neuronal culture and transfection
  - Preparation of ESC-derived human iNs and transduction of ASAP5-Kv
  - Lentivirus plasmid construction and packaging for human iNs experiments
  - Animals
- **METHOD DETAILS**
  - Plasmid construction
  - Cell screening
  - Whole-cell patch-clamping and imaging of HEK293A cells
  - Electrophysiology and voltage imaging from cultured neurons
  - Detecting mEPSPs at the soma in cultured neurons
  - Mapping the propagation of mEPSPs in cultured neurons
  - Brightness comparison in cultured neurons
  - One-photon voltage imaging in mouse and sensor comparison
  - One-photon voltage imaging in zebrafish
  - Two-photon *in vivo* imaging of *Drosophila*
  - Two-photon *in vivo* voltage imaging in mouse motor cortex
  - Two-photon *in vivo* voltage imaging in mouse visual cortex in behaving mice
  - Two-photon *in vivo* imaging in barrel cortex
- **QUANTIFICATION AND STATISTICAL ANALYSIS**

**SUPPLEMENTAL INFORMATION**

Supplemental information can be found online at <https://doi.org/10.1016/j.neuron.2024.08.019>.

Received: October 10, 2023

Revised: July 23, 2024

Accepted: August 27, 2024

Published: September 20, 2024

**REFERENCES**

1. Bean, B.P. (2007). The action potential in mammalian central neurons. *Nat. Rev. Neurosci.* 8, 451–465. <https://doi.org/10.1038/nrn2148>.
2. Fatt, P., and Katz, B. (1952). Spontaneous subthreshold activity at motor nerve endings. *J. Physiol.* 117, 109–128. <https://doi.org/10.1113/jphysiol.1952.sp004735>.
3. Häusser, M., Spruston, N., and Stuart, G.J. (2000). Diversity and dynamics of dendritic signaling. *Science* 290, 739–744. <https://doi.org/10.1126/science.290.5492.739>.
4. Südhof, T.C. (2018). Towards an Understanding of Synapse Formation. *Neuron* 100, 276–293. <https://doi.org/10.1016/j.neuron.2018.09.040>.
5. Pak, C., Danko, T., Zhang, Y., Aoto, J., Anderson, G., Maxeiner, S., Yi, F., Wernig, M., and Südhof, T.C. (2015). Human Neuropsychiatric Disease Modeling using Conditional Deletion Reveals Synaptic Transmission Defects Caused by Heterozygous Mutations in NRXN1. *Cell Stem Cell* 17, 316–328. <https://doi.org/10.1016/j.stem.2015.07.017>.
6. Bardy, C., van den Hurk, M., Kakaradov, B., Erwin, J.A., Jaeger, B.N., Hernandez, R.V., Eames, T., Paucar, A.A., Gorris, M., Marchand, C., et al. (2016). Predicting the functional states of human iPSC-derived neurons with single-cell RNA-seq and electrophysiology. *Mol. Psychiatry* 21, 1573–1588. <https://doi.org/10.1038/mp.2016.158>.
7. Christian, K.M., Song, H., and Ming, G.L. (2020). Using Two- and Three-Dimensional Human iPSC Culture Systems to Model Psychiatric Disorders. *Adv. Neurobiol.* 25, 237–257. [https://doi.org/10.1007/978-3-030-45493-7\\_9](https://doi.org/10.1007/978-3-030-45493-7_9).
8. Page, S.C., Sripathy, S.R., Farinelli, F., Ye, Z., Wang, Y., Hiler, D.J., Pattie, E.A., Nguyen, C.V., Tippani, M., Moses, R.L., et al. (2022). Electrophysiological measures from human iPSC-derived neurons are associated with schizophrenia clinical status and predict individual cognitive performance. *Proc. Natl. Acad. Sci. USA* 119, e2109395119. <https://doi.org/10.1073/pnas.2109395119>.
9. Evans, S.W., Shi, D.Q., Chavarha, M., Plitt, M.H., Taxidis, J., Madruga, B., Fan, J.L., Hwang, F.J., van Keulen, S.C., Suomivuori, C.M., et al. (2023). A positively tuned voltage indicator for extended electrical recordings in the brain. *Nat. Methods* 20, 1104–1113. <https://doi.org/10.1038/s41592-023-01913-z>.
10. Liu, Z., Lu, X., Villette, V., Gou, Y., Colbert, K.L., Lai, S., Guan, S., Land, M.A., Lee, J., Assefa, T., et al. (2022). Sustained deep-tissue voltage recording using a fast indicator evolved for two-photon microscopy. *Cell* 185, 3408–3425.e29. <https://doi.org/10.1016/j.cell.2022.07.013>.
11. Kannan, M., Vasan, G., Haziza, S., Huang, C., Chrapkiewicz, R., Luo, J., Cardin, J.A., Schnitzer, M.J., and Pieribone, V.A. (2022). Dual-polarity voltage imaging of the concurrent dynamics of multiple neuron types. *Science* 378, eabm8797. <https://doi.org/10.1126/science.abm8797>.
12. Cornejo, V.H., Ofer, N., and Yuste, R. (2022). Voltage compartmentalization in dendritic spines *in vivo*. *Science* 375, 82–86. <https://doi.org/10.1126/science.abg0501>.
13. Bowman, A.J., Huang, C., Schnitzer, M.J., and Kasevich, M.A. (2023). Wide-field fluorescence lifetime imaging of neuron spiking and subthreshold activity *in vivo*. *Science* 380, 1270–1275. <https://doi.org/10.1126/science.adf9725>.
14. Villette, V., Chavarha, M., Dimov, I.K., Bradley, J., Pradhan, L., Mathieu, B., Evans, S.W., Chamberland, S., Shi, D., Yang, R., et al. (2019). Ultrafast Two-Photon Imaging of a High-Gain Voltage Indicator in Awake Behaving Mice. *Cell* 179, 1590–1608.e23. <https://doi.org/10.1016/j.cell.2019.11.004>.
15. Abdelfattah, A.S., Zheng, J., Singh, A., Huang, Y.C., Reep, D., Tsegaye, G., Tsang, A., Arthur, B.J., Rehorova, M., Olson, C.V.L., et al. (2023). Sensitivity optimization of a rhodopsin-based fluorescent voltage indicator. *Neuron* 111, 1547–1563.e9. <https://doi.org/10.1016/j.neuron.2023.03.009>.

16. Lu, X., Wang, Y., Liu, Z., Gou, Y., Jaeger, D., and St-Pierre, F. (2023). Widefield imaging of rapid pan-cortical voltage dynamics with an indicator evolved for one-photon microscopy. *Nat. Commun.* 14, 6423. <https://doi.org/10.1038/s41467-023-41975-3>.
17. Behnia, R., Clark, D.A., Carter, A.G., Clandinin, T.R., and Desplan, C. (2014). Processing properties of ON and OFF pathways for *Drosophila* motion detection. *Nature* 512, 427–430. <https://doi.org/10.1038/nature13427>.
18. Yang, H.H., St-Pierre, F., Sun, X., Ding, X., Lin, M.Z., and Clandinin, T.R. (2016). Subcellular Imaging of Voltage and Calcium Signals Reveals Neural Processing In Vivo. *Cell* 166, 245–257. <https://doi.org/10.1016/j.cell.2016.05.031>.
19. Frank, D.D., Jouandet, G.C., Kearney, P.J., Macpherson, L.J., and Gallio, M. (2015). Temperature representation in the *Drosophila* brain. *Nature* 519, 358–361. <https://doi.org/10.1038/nature14284>.
20. Alpert, M.H., Frank, D.D., Kaspi, E., Flourakis, M., Zaharieva, E.E., Allada, R., Para, A., and Gallio, M. (2020). A Circuit Encoding Absolute Cold Temperature in *Drosophila*. *Curr. Biol.* 30, 2275–2288.e5. <https://doi.org/10.1016/j.cub.2020.04.038>.
21. Wu, J., Liang, Y., Chen, S., Hsu, C.L., Chavarha, M., Evans, S.W., Shi, D., Lin, M.Z., Tsia, K.K., and Ji, N. (2020). Kilohertz two-photon fluorescence microscopy imaging of neural activity in vivo. *Nat. Methods* 17, 287–290. <https://doi.org/10.1038/s41592-020-0762-7>.
22. Moore, C.I., and Nelson, S.B. (1998). Spatio-temporal subthreshold receptive fields in the vibrissa representation of rat primary somatosensory cortex. *J. Neurophysiol.* 80, 2882–2892. <https://doi.org/10.1152/jn.1998.80.6.2882>.
23. Brecht, M., Roth, A., and Sakmann, B. (2003). Dynamic receptive fields of reconstructed pyramidal cells in layers 3 and 2 of rat somatosensory barrel cortex. *J. Physiol.* 553, 243–265. <https://doi.org/10.1113/jphysiol.2003.044222>.
24. Crochet, S., Poulet, J.F.A., Kremer, Y., and Petersen, C.C.H. (2011). Synaptic mechanisms underlying sparse coding of active touch. *Neuron* 69, 1160–1175. <https://doi.org/10.1016/j.neuron.2011.02.022>.
25. Froemke, R.C. (2015). Plasticity of cortical excitatory-inhibitory balance. *Annu. Rev. Neurosci.* 38, 195–219. <https://doi.org/10.1146/annurev-neuro-071714-034002>.
26. Zhou, B., Lu, J.G., Siddu, A., Wernig, M., and Südhof, T.C. (2022). Synaptogenic effect of APP-Swedish mutation in familial Alzheimer's disease. *Sci. Transl. Med.* 14, eabn9380. <https://doi.org/10.1126/scitranslmed.abn9380>.
27. Pernía-Andrade, A.J., Goswami, S.P., Stickler, Y., Fröbe, U., Schlägl, A., and Jonas, P. (2012). A deconvolution-based method with high sensitivity and temporal resolution for detection of spontaneous synaptic currents in vitro and in vivo. *Biophys. J.* 103, 1429–1439. <https://doi.org/10.1016/j.biophys.2012.08.039>.
28. Wilt, B.A., Fitzgerald, J.E., and Schnitzer, M.J. (2013). Photon shot noise limits on optical detection of neuronal spikes and estimation of spike timing. *Biophys. J.* 104, 51–62. <https://doi.org/10.1016/j.biophys.2012.07.058>.
29. O'Neill, P.S., Baccino-Calace, M., Rupprecht, P., Friedrich, R.W., Müller, M., and Delvendahl, I. (2023). A deep learning framework for automated and generalized synaptic event analysis. Preprint at eLife. <https://doi.org/10.7554/eLife.98485.1>.
30. Magee, J.C. (2000). Dendritic integration of excitatory synaptic input. *Nat. Rev. Neurosci.* 1, 181–190. <https://doi.org/10.1038/35044552>.
31. Segev, I., and London, M. (2000). Untangling dendrites with quantitative models. *Science* 290, 744–750. <https://doi.org/10.1126/science.290.5492.744>.
32. Williams, S.R., and Stuart, G.J. (2002). Dependence of EPSP efficacy on synapse location in neocortical pyramidal neurons. *Science* 295, 1907–1910. <https://doi.org/10.1126/science.1067903>.
33. Li, B., Sutari, B.S., Sun, S.D., Luo, Z., Wei, C., Chenouard, N., Mandelberg, N.J., Zhang, G., Wamsley, B., Tian, G., et al. (2020). Neuronal Inactivity Co-opts LTP Machinery to Drive Potassium Channel Splicing and Homeostatic Spike Widening. *Cell* 181, 1547–1565.e15. <https://doi.org/10.1016/j.cell.2020.05.013>.
34. Nevian, T., Larkum, M.E., Polksy, A., and Schiller, J. (2007). Properties of basal dendrites of layer 5 pyramidal neurons: a direct patch-clamp recording study. *Nat. Neurosci.* 10, 206–214. <https://doi.org/10.1038/nn1826>.
35. Koch, C. (2004). *Biophysics of Computation: Information Processing in Single Neurons* 588 (Oxford Academic).
36. Culotta, L., and Penzes, P. (2020). Exploring the mechanisms underlying excitation/inhibition imbalance in human iPSC-derived models of ASD. *Mol. Autism* 11, 32. <https://doi.org/10.1186/s13229-020-00339-0>.
37. Williams, L.A., Joshi, V., Murphy, M., Ferrante, J., Werley, C.A., Brookings, T., McManus, O., Grosse, J., Davies, C.H., and Dempsey, G.T. (2019). Scalable Measurements of Intrinsic Excitability in Human iPS Cell-Derived Excitatory Neurons Using All-Optical Electrophysiology. *Neurochem. Res.* 44, 714–725. <https://doi.org/10.1007/s11064-018-2694-5>.
38. Alich, T.C., Röderer, P., Szalontai, B., Golcuk, K., Tariq, S., Peitz, M., Brüstle, O., and Mody, I. (2022). Bringing to light the physiological and pathological firing patterns of human induced pluripotent stem cell-derived neurons using optical recordings. *Front. Cell. Neurosci.* 16, 1039957. <https://doi.org/10.3389/fncel.2022.1039957>.
39. Puppo, F., Sadegh, S., Trujillo, C.A., Thunemann, M., Campbell, E.P., Vandenbergh, M., Shan, X., Akkouh, I.A., Miller, E.W., Bloodgood, B.L., et al. (2021). All-Optical Electrophysiology in hiPSC-Derived Neurons With Synthetic Voltage Sensors. *Front. Cell. Neurosci.* 15, 671549. <https://doi.org/10.3389/fncel.2021.671549>.
40. Zhang, Y., Pak, C., Han, Y., Ahlenius, H., Zhang, Z., Chanda, S., Marro, S., Patzke, C., Acuna, C., Covy, J., et al. (2013). Rapid single-step induction of functional neurons from human pluripotent stem cells. *Neuron* 78, 785–798. <https://doi.org/10.1016/j.neuron.2013.05.029>.
41. Pak, C., Danko, T., Mirabella, V.R., Wang, J., Liu, Y., Vangipuram, M., Grieder, S., Zhang, X., Ward, T., Huang, Y.A., et al. (2021). Cross-platform validation of neurotransmitter release impairments in schizophrenia patient-derived NRXN1-mutant neurons. *Proc. Natl. Acad. Sci. USA* 118, e2025598118. <https://doi.org/10.1073/pnas.2025598118>.
42. Weber, T.D., Moya, M.V., Kılıç, K., Mertz, J., and Economo, M.N. (2023). High-speed multiplane confocal microscopy for voltage imaging in densely labeled neuronal populations. *Nat. Neurosci.* 26, 1642–1650. <https://doi.org/10.1038/s41593-023-01408-2>.
43. Brinks, D., Klein, A.J., and Cohen, A.E. (2015). Two-Photon Lifetime Imaging of Voltage Indicating Proteins as a Probe of Absolute Membrane Voltage. *Biophys. J.* 109, 914–921. <https://doi.org/10.1016/j.biophys.2015.07.038>.
44. Rhee, J.K., Leong, L.M., Mukim, M.S.I., Kang, B.E., Lee, S., Bilbao-Broch, L., and Baker, B.J. (2020). Biophysical Parameters of GEVLs: Considerations for Imaging Voltage. *Biophys. J.* 119, 1–8. <https://doi.org/10.1016/j.biophys.2020.05.019>.
45. Hou, J.H., Venkatachalam, V., and Cohen, A.E. (2014). Temporal dynamics of microbial rhodopsin fluorescence reports absolute membrane voltage. *Biophys. J.* 106, 639–648. <https://doi.org/10.1016/j.biophys.2013.11.4493>.
46. Silapetere, A., Hwang, S., Hontani, Y., Fernandez Lahore, R.G., Balke, J., Escobar, F.V., Tros, M., Konold, P.E., Matis, R., Croce, R., et al. (2022). QuasAr Odyssey: the origin of fluorescence and its voltage sensitivity in microbial rhodopsins. *Nat. Commun.* 13, 5501. <https://doi.org/10.1038/s41467-022-33084-4>.
47. Lam, A.J., St-Pierre, F., Gong, Y., Marshall, J.D., Cranfill, P.J., Baird, M.A., McKeown, M.R., Wiedenmann, J., Davidson, M.W., Schnitzer, M.J., et al. (2012). Improving FRET dynamic range with bright green and red fluorescent proteins. *Nat. Methods* 9, 1005–1012. <https://doi.org/10.1038/nmeth.2171>.

48. Zhang, D.Y., Lau, C.P., and Li, G.R. (2009). Human Kir2.1 channel carries a transient outward potassium current with inward rectification. *Pflugers Arch.* **457**, 1275–1285. <https://doi.org/10.1007/s00424-008-0608-0>.
49. Tuthill, J.C., Nern, A., Holtz, S.L., Rubin, G.M., and Reiser, M.B. (2013). Contributions of the 12 neuron classes in the fly lamina to motion vision. *Neuron* **79**, 128–140. <https://doi.org/10.1016/j.neuron.2013.05.024>.
50. Cai, C., Friedrich, J., Singh, A., Eybposh, M.H., Pnevmatikakis, E.A., Podgorski, K., and Giovannucci, A. (2021). VoIPy: Automated and scalable analysis pipelines for voltage imaging datasets. *PLoS Comput. Biol.* **17**, e1008806. <https://doi.org/10.1371/journal.pcbi.1008806>.
51. Essayan-Perez, S., and Südhof, T.C. (2023). Neuronal  $\gamma$ -secretase regulates lipid metabolism, linking cholesterol to synaptic dysfunction in Alzheimer's disease. *Neuron* **111**, 3176–3194.e7. <https://doi.org/10.1016/j.neuron.2023.07.005>.
52. Hwang, F.J., Roth, R.H., Wu, Y.W., Sun, Y., Kwon, D.K., Liu, Y., and Ding, J.B. (2022). Motor learning selectively strengthens cortical and striatal synapses of motor engram neurons. *Neuron* **110**, 2790–2801.e5. <https://doi.org/10.1016/j.neuron.2022.06.006>.
53. Thévenaz, P., Ruttmann, U.E., and Unser, M. (1998). A pyramid approach to subpixel registration based on intensity. *IEEE Trans. Image Process.* **7**, 27–41. <https://doi.org/10.1109/83.650848>.
54. Turner, M.H., Krieger, A., Pang, M.M., and Clandinin, T.R. (2022). Visual and motor signatures of locomotion dynamically shape a population code for feature detection in *Drosophila*. *eLife* **11**, e82587. <https://doi.org/10.7554/eLife.82587>.
55. Villette, V., Levesque, M., Miled, A., Gosselin, B., and Topolini, L. (2017). Simple platform for chronic imaging of hippocampal activity during spontaneous behaviour in an awake mouse. *Sci. Rep.* **7**, 43388. <https://doi.org/10.1038/srep43388>.
56. Drew, P.J., and Feldman, D.E. (2009). Intrinsic signal imaging of deprivation-induced contraction of whisker representations in rat somatosensory cortex. *Cereb. Cortex* **19**, 331–348. <https://doi.org/10.1093/cercor/bhn085>.
57. Fan, J.L., Rivera, J.A., Sun, W., Peterson, J., Haeberle, H., Rubin, S., and Ji, N. (2020). High-speed volumetric two-photon fluorescence imaging of neurovascular dynamics. *Nat. Commun.* **11**, 6020. <https://doi.org/10.1038/s41467-020-19851-1>.
58. Pnevmatikakis, E.A., and Giovannucci, A. (2017). NoRMCorre: An online algorithm for piecewise rigid motion correction of calcium imaging data. *J. Neurosci. Methods* **291**, 83–94. <https://doi.org/10.1016/j.jneumeth.2017.07.031>.
59. Giovannucci, A., Friedrich, J., Gunn, P., Kalfon, J., Brown, B.L., Koay, S.A., Taxidis, J., Najafi, F., Gauthier, J.L., Zhou, P., et al. (2019). CalmAn an open source tool for scalable calcium imaging data analysis. *eLife* **8**, e38173. <https://doi.org/10.7554/eLife.38173>.

## STAR★METHODS

## KEY RESOURCES TABLE

REAGENT or RESOURCE	SOURCE	IDENTIFIER
<b>Bacterial and virus strains</b>		
AAV1.hSyn::Cre.WPRE	UPENN vector core	Addgene 105553-AAV1
AAV9. CamKII 0.4::Cre.SV40	UPENN vector core	Addgene 105558-AAV9
AAV9.hSyn::ASAP5-Kv.WPRE	This paper	N/A
AAV9.EF1a:DIO:ASAP5-Kv.WPRE	This paper	Stanford GVVC-AAV-302
<b>Chemicals, peptides, and recombinant proteins</b>		
Lipofectamine 2000	ThermoFisher	Cat#11668027
Lipofectamine 3000	ThermoFisher	Cat#L3000001
JaneliaFluor 525	Promega	Cat#CS315102
<b>Experimental models: Cell lines</b>		
HEK293A	ThermoFisher	Cat# R70507
HEK293-Kir2.1	Zhang et al. <sup>48</sup>	N/A
<b>Experimental models: Organisms/strains</b>		
C57-BL6 (wild-type) mouse	Jackson Labs	Strain # 000664
Sprague Dawley (wild-type) rat	Charles River	Sprague Dawley
+; UAS-ASAP5 (Attp40)/CyO; UAS-jRGECO1a (vk00005)/Tm6B	This paper	BDSC #605338
+; +; GMR19F01-GAL4	Bloomington Drosophila Stock Center (BDSC)	Stock # 48852
+; 53G02-AD; 29G11-DBD	Tuthill et al. <sup>49</sup>	N/A
+; +; GMR60H12-GAL4	BDSC	Stock # 39268
<b>Recombinant DNA</b>		
pAAV.hSyn::ASAP5-Kv.WPRE	This paper	Addgene: 225707
pAAV.hSyn::ASAP5.WPRE	This paper	Addgene: 225709
pAAV.EF1a:DIO:ASAP5-Kv.WPRE	This paper	Addgene: 225708
<b>Software and algorithms</b>		
Python3.10	Python Software Foundation	RRID:SCR_008394
MATLAB R2021b	Mathworks	RRID:SCR_001622
Prism 10	GraphPad	RRID:SCR_002798
Volpy	Cai et al. <sup>50</sup>	<a href="https://github.com/caichangjia/VolPy">https://github.com/caichangjia/VolPy</a>
HClImage Live	Hamamatsu Photonics	RRID:SCR_015041
<b>Other</b>		
Custom-designed AOD-based RAMP microscope + ULoVE module	Karthala Systems (France)	N/A
Femto 3D Atlas Plug & Play	Femtonics (Hungary)	N/A

## EXPERIMENTAL MODEL AND STUDY PARTICIPANT DETAILS

## Cultured cell lines

For electroporation-based screening, the previously described HEK293-Kir2.1 cell line was maintained in high-glucose DMEM (Thermo Fisher Scientific, 31053036), 5% FBS (Gemini Bio), 2 mM L-glutamine (Gemini Bio) and 500 µg/mL geneticin (Thermo Fisher Scientific, 10131035). For electrophysiological recordings to measure the responsivity and kinetics of voltage indicators, HEK293A cells (Thermo Fisher Scientific, R70507) were cultured in high-glucose DMEM with 5% FBS and 2 mM L-glutamine. All cell lines were maintained in a humidified incubator at 37°C with 5% CO<sub>2</sub>.

### Primary neuronal culture and transfection

Primary culture of rat neurons and transfection were conducted as previously described.<sup>9</sup> Briefly, hippocampus and cortex from embryonic day 18 Sprague Dawley rat's brain were dissected separately and dissociated in TrypLE Select enzyme (Gibco) mixed with 0.005% DNaseI. The dissociated neurons were seeded at 70,000 hippocampal cells/well or 100,000 cortical cells/well (500- $\mu$ L working volume per well) on poly-D-lysine (0.1 mg/mL; Gibco) coated round coverslips (12-mm diameter and 0.13–0.17-mm thick coverslips; Carolina biological). At 9–12 days in vitro (DIV), the neurons were transfected with 100–200 ng of GEVI plasmid under the hSyn promoter using Lipofectamine 2000 (Invitrogen). For the dendritic mEPSP mapping experiment (see below), the rat cortical neurons were cultured on 24-well glass-bottom plates (0.170  $\pm$  0.005 mm thick cover-glass; CellVis) at the same density as described above. The transfection was done at 16 DIV. All the neurons were maintained until the day of imaging by performing a half-media change per well on every 3<sup>rd</sup> day, for example, on 1, 4, 7, 10, 13, 16, 19, 22, and 25 DIV with fresh Neurobasal media supplemented with 2 % v/v B-27 and 2 mM GlutaMax (all from Gibco). Primary neuronal culture was maintained in a humidified incubator at 37 °C with 5% CO<sub>2</sub>.

### Preparation of ESC-derived human iNs and transduction of ASAP5-Kv

H1 ESCs were maintained in mTeSR1 medium (Stem Cell Technologies). Human induced neurons were generated from H1 ESCs as previously described<sup>40</sup> with a few modifications. On the day of induction, ES cells were treated with Accutase, plated as dissociated cells on matrigel-coated wells in mTeSR1 medium containing 2  $\mu$ M thiazovivin, and infected with TetO-Puro-Ngn2 and rtTA (3.5  $\mu$ L for each well in a 6-well plate) lentivirus particles prepared as described above. On day 1, doxycycline (2 mg/L, Sigma) was added to the induction media (Non-Essential Amino Acids, BDNF (10 ng/ml, PeproTech), human NT3 (10 ng/ml, PeproTech) and mouse Laminin-1 (0.2  $\mu$ g/ml, PeproTech)) to induce TetO gene expression. On days 2 and 3, puromycin (1 mg/L) was added to the induction media to select only previously infected cells. On day 4, iN cells were dissociated with Accutase and plated 100,000 cells/well on a 24-well plate in Neurobasal media with Gem21 (Gemini bio), doxycycline, BDNF, NT3, Laminin-1, and Glutamax. On day 5, 2.3  $\mu$ L of ASAP5-Kv lentivirus was added to each well of a 24-well plate and on day-6, glial cells (cultured from forebrain of newborn wildtype CD1 mice) were added. On days 7 and 9, 4Ara-C (2  $\mu$ M, Sigma) was added to the medium to inhibit astrocyte proliferation. From day 10, 5% FBS was added to the medium. Since then, a half of the medium in each well was changed weekly. The human iNs were then used for experiments on days 30–80. All human iNs were maintained in a humidified incubator at 37 °C with 5% CO<sub>2</sub>.

### Lentivirus plasmid construction and packaging for human iNs experiments

Lentivirus constructs for induction of human neurons from H1 ESCs were prepared as previously described.<sup>40</sup> Briefly, Rev, RRE, and VSV helper plasmids were used for lentiviral packaging of Ngn2 and rtTA. Additionally, ASAP5-Kv was packaged with either hSyn or Ubiquitin-C promoter to express the GEVI into human iNs.

All lentiviruses were packaged using HEK293T cells (ATCC) as previously described.<sup>51</sup> Briefly, lentiviral vector plasmid (12  $\mu$ g) and helper plasmids (4  $\mu$ g Rev, 8  $\mu$ g RRE, and 6  $\mu$ g VSVG) were co-transfected in T75 flask by the calcium phosphate method. Lentivirus particles were harvested from the medium 48 h after transfection. To concentrate viral particles, supernatant was pelleted by centrifugation at 19,000 g for 2 h, resuspended in DMEM, and frozen in aliquots at –80 °C.

### Animals

All flies used for imaging were raised on standard molasses food at 25 °C on a 12/12-h light-dark cycle. ASAP5 was inserted into the attP40 phiC31 landing site by injection of a pJFRC7-20XUAS-ASAP5 plasmid (BestGene). We used the cell-type-specific driver GMR19F01-Gal4 to express GEVIs in Mi1, 53G02AD-29G11DBD split-Gal4 to express GEVIs in L2 neurons, and R60H12-Gal4 to express ASAP5 in TPN-II neurons. Female flies of the appropriate genotypes were collected on day 2 and imaged at room temperature (20 °C) on day 5 post eclosion. The genotypes of the imaged flies in Figures 3 and S3 were:

Mi1»JEDI-2P: +/+; UAS-JEDI-2P/+; UAS-jRGECO1a /GMR19F01-Gal4  
 Mi1»ASAP5: +/+; UAS-ASAP5/+; UAS-jRGECO1a /GMR19F01-Gal4  
 L2»JEDI-2P: +/+; UAS-JEDI-2P/53G02-AD; UAS-jRGECO1a/29G11-DBD  
 L2»ASAP5: +/+; UAS-ASAP5/53G02-AD; UAS-jRGECO1a/29G11-DBD  
 TPN-II»ASAP5: +/+; UAS-ASAP5/+ ; R60H12-Gal4/+

For rat hippocampal and cortical neuronal culture, Sprague Dawley rat embryos at embryonic day 18 were obtained with approval by the Stanford Institutional Animal Use and Care Committee. Male and female rats were used interchangeably.

For *in vivo* experiments in mouse motor cortex, wild-type C57BL/6 mice (P51-101) were used with procedures approved by the Stanford Institutional Animal Use and Care Committee. Male and female mice were used interchangeably for the experiment. The mice were 8–14 weeks-old at the time of viral injection. For *in vivo* experiments in mouse barrel cortex, all animal procedures were approved by the UC Berkeley Animal Care and Use Committee and followed NIH guidelines. Prior to surgery, mice were housed in cohorts of 3–4 in reverse 12/12-hour light-dark cycles with humidity 30–70% and temperature 20–26 °C. Male and female mice were used interchangeably for the experiment. The mice were 8–12 weeks-old at the time of viral injection. All behavioral training and imaging experiments were conducted in the dark cycle. Mice were singly housed in separate cages with running wheels after

performing cranial window surgery and mounting head fixation gear. Drd3-Cre mice were used with viral expression of ASAP5-Kv under the hSyn promoter, which achieved neuron specific expression of ASAP5-Kv in S1. For *in vivo* experiments in mouse visual cortex, all protocols adhered to the guidelines of the French National Ethics Committee for Sciences and Health report on Ethical Principles for Animal Experimentation in agreement with the European Community Directive 86/609/EEC under agreement #29791. 6 male wildtype C57BL/6J adult mice (>P40 - body weight 20–24 g) were housed in standard conditions (12-h light/dark cycles, light on at 7 a.m., with water and food ad libitum). A preoperative analgesic was used (buprenorphine, 0.1 mg/kg), and Ketamine-Xylazine were used as anesthetic (Centravet).

## METHOD DETAILS

### Plasmid construction

For electroporation-based screening in HEK293-Kir2.1 cells, the ASAP3 genes with designed mutations were cloned into pcDNA3.1 with a CMV enhancer and promoter and bGH poly(A) signal. For patch-clamp characterization in HEK293A cells, all voltage indicators were subcloned into a pcDNA3.1/Puro-CAG vector between NheI and HindIII sites.

For *in vitro* characterization in cultured neurons, ASAP5 was subcloned into pAAV-hSyn-WPRE. For making transgenic fly lines, ASAP5 was cloned into pJFRC7-20XUAS vector. For *in vivo* mouse voltage imaging, ASAP5-Kv was cloned into pAAV-hSyn-WPRE or pAAV-EF1 $\alpha$ -Dio-WPRE, and then packaged into AAV9 capsids by the Neuroscience Gene Vector and Virus Core (GVVC) at Stanford University. For somatic targeting expression *in vivo*, a 65-amino-acid cytoplasmic segment of Kv2.1 potassium channel was added to the C terminus of ASAP5 followed by an LKGSSGSSGSSTR linker. All plasmids were made by standard molecular biology techniques with all cloned fragments or whole plasmids confirmed by sequencing (Sequetech and Primordium labs).

For the comparison with Voltron2 in cultured neurons, we cloned pAAV-hSyn-Voltron2-Kv-WPRE by taking the Voltron2, the Golgi export trafficking sequence, and the endoplasmic reticulum export sequence (ER) from pGP-pcDNA3.1 Puro-CAG-Voltron2-ST plasmid. Then, the fragment was inserted into a pAAV-hSyn-WPRE backbone vector together with the soma-targeting tag from Kv2.1 by using In-Fusion HD cloning kit (Takara). pGP-pcDNA3.1 Puro-CAG-Voltron2-ST was a gift from GENIE Project (RRID: Addgene\_172910).

### Cell screening

HEK293-Kir2.1 cells were screened in 384-well plates (Grace Bio-Labs) on conductive glass slides (Sigma-Aldrich) with customized electrophoresis-based screening system. 2 days before imaging, cells were transfected with PCR-generated libraries with Lipofectamine 3000 followed by a media change after 6 h. Cells were imaged at room temperature on an IX81 inverted microscope (Olympus). A blue LED (Prizmatix UHP-Mic-LED-460) passed through a 480/40-nm excitation filter and focused on the sample through a  $\times 20$  0.75-NA objective (Olympus). Emitted fluorescence was passed through a 503-nm long-pass emission filter. A single FOV was imaged for a total of 3 s with a 10- $\mu$ s 150-V electrical square pulse applied. Images were recorded at 300 fps by an ORCA Flash4.0 V2 CMOS camera (Hamamatsu, C11440-22CA) with pixel binning set to  $4 \times 4$ . All operations were controlled by a customized software in MATLAB (MathWorks).

### Whole-cell patch-clamping and imaging of HEK293A cells

Cells were transfected with pcDNA3.1/Puro-CAG-based plasmids expressing each GEVI using Lipofectamine 3000 in 24-well plates following the manufacturer's recommended instructions. 30 h after being plated on 12-mm glass coverslips (Carolina Biological), the cells were voltage-clamped (Multiclamp 700B amplifier with pClamp software, Molecular Devices) and recorded by an iXon 860 EMCCD camera (Oxford Instruments) with a  $\times 40$  1.3-NA oil-immersion objective (Zeiss). Blue light from a UHP-F-455 LED (Prizmatix) served as the excitation light source. The filter cube set consisted of a 484/15-nm excitation filter and a 525/50-nm emission filter. The power density at the sample was 20–41 mW/mm<sup>2</sup>.

To characterize the fluorescence-voltage curve of the indicators, cells were clamped at a baseline potential of -70 mV, then 400 ms of voltage steps at -200, -160, -140, -120, -100, -80, -70, -60, -40, -20, 0, 30, 50, 80 mV followed by 400 ms of -70 mV baseline. To characterize the response of voltage indicators to action potentials, a scaled AP waveform (FWHM 2.0 ms or 4.0 ms, -70 mV to +30 mV) recorded from a cultured hippocampal neuron was applied to HEK293A cells.

To characterize kinetics of ASAP indicators at both 22°C and 37°C, a 30-mV voltage step was applied to cells from -70 mV baseline and images were acquired at 1888 fps. Time constants were obtained using MATLAB curve fitting (MathWorks).

### Electrophysiology and voltage imaging from cultured neurons

All electrophysiological recordings were conducted with Multiclamp 700B amplifier, Digidata 1440A digitizer, and pClamp software (all from Molecular devices). Glass capillaries with filament having 1.5 mm outer diameter, 1.0 mm inner diameter and 75 mm axial length (King Precision Glass) were used for whole-cell voltage and current clamp recordings. Recordings from cultured rat neurons and human iPSCs were conducted at room temperature under similar conditions described in a previously reported paper.<sup>41</sup> The pipette solution contained 123 mM K-gluconate, 10 mM KCl, 8 mM NaCl, 1 mM MgCl<sub>2</sub>, 10 mM HEPES, 1 mM EGTA, 0.1 mM CaCl<sub>2</sub>, 1.5 mM MgATP, 0.2 mM Na<sub>4</sub>GTP, and 4 mM glucose, and the pH was adjusted to 7.2 with KOH. Osmolarity was 295–300 mOsm/kg. The resistance of intracellular solution filled pipettes was 3–5 MΩ. The extracellular solution contained 145 mM NaCl, 3 mM KCl,

2 mM CaCl<sub>2</sub>, 2 mM MgCl<sub>2</sub>, 10 mM HEPES, and 10 mM glucose, and the pH was adjusted to 7.4 with NaOH. Osmolarity was 310 mOsm/kg. Whole-cell current clamp recordings requiring more than  $\pm$  100 pA holding current to maintain resting membrane potential near -70 mV were excluded from analysis. Tetrodotoxin (TTX; 1  $\mu$ M) and picrotoxin (PTX; 50  $\mu$ M) were added to the bath solution to isolate miniature excitatory postsynaptic activity. To remove AMPA-receptor dependent miniature events, 6-cyano-7-nitroquinoxaline-2,3-dione (CNQX; 20  $\mu$ M) was added to the bath solution. Electrophysiological recordings were acquired at 10 kHz sampling rate, but they were resampled to 0.4 or 1 kHz for visualization in the figures. Clampfit 11 (Molecular devices) was used for post-processing and analyses of all recordings. For detection of miniature EPSPs in Figure 7C, the template search function in Clampfit 11 was first used, and then detected events were further sorted with a minimum threshold of 0.5 mV followed by a visual inspection of each event.

For voltage imaging of cultured neurons, the blue light from UHP-F-455 LED (Prizmatix) was filtered through a 482/18-nm bandpass filter (Semrock) and focused by a  $\times$ 40 1.3-NA oil-immersion objective lens (Zeiss). The power density at the sample ranged from 56 to 92 mW/mm<sup>2</sup>. The resulting fluorescence emission filtered by a 525/50 nm bandpass filter (Semrock) was imaged on a sCMOS camera (Flash4-V2 C11440-22CU, Hamamatsu) with various sub-array sizes to achieve suitable frame rate for each experiment. For voltage imaging of spontaneous activity from the two rat hippocampal neurons shown in Figure S6C, HBSS solution containing 10 mM HEPES, 2 mM GlutaMax, and 1 mM sodium pyruvate was used. The excitation was delivered by a 20x objective lens (NA 1.0, Olympus) and the power density at the sample was 70 mW/mm<sup>2</sup>. Photobleaching in resulting fluorescence traces was corrected by normalizing with exponential decay function using MATLAB. Fluorescence traces in Figures 7C and S6B were lowpass filtered with passband frequency of 80 Hz in MATLAB. The sCMOS camera (Flash4-V2 C11440-22CU, Hamamatsu) we used for the dendritic EPSPs voltage imaging result in Figure 6A acquires signal with rolling shutter, which causes time delay in y-axis of the image. Since the result compared time-series signal from multiple ROIs, we corrected for the delay in different rows by using digital interpolation.

For Voltron2-Kv expressing neurons, JaneliaFluor 525 (JF525) - HaloTag ligands (Item No: CS315102; Promega) were added prior to experiments following the procedures described in the original literature<sup>15</sup> and by the manufacturer. Briefly, the neurons were gently rinsed with the extracellular bath solution. Then, JF525-HaloTag ligands were added to each well at 100 nM concentration. After 10 min of incubation, the neurons were washed twice with the extracellular solution.

To compare ASAP5-Kv and Voltron2-Kv for optical detection of mEPSPs, cultured rat hippocampal neurons at 14–21 DIV were patched and imaged simultaneously. For electrophysiological recordings, extracellular solution containing 145 mM NaCl, 3 mM KCl, 2 mM CaCl<sub>2</sub>, 2 mM MgCl<sub>2</sub>, 10 mM HEPES, and 10 mM glucose (pH adjusted to 7.4) supplemented with TTX (1  $\mu$ M) and PTX (50  $\mu$ M), and the pipette solution containing 123 mM K-gluconate, 10 mM KCl, 8 mM NaCl, 1 mM MgCl<sub>2</sub>, 10 mM HEPES, 1 mM EGTA, 0.1 mM CaCl<sub>2</sub>, 1.5 mM MgATP, 0.2 mM Na<sub>4</sub>GTP, and 4 mM glucose (pH adjusted to 7.2) were used. The excitation for ASAP5-Kv was provided by SOLIS-470C LED (Thorlabs), filtered by a 482/18-nm bandpass filter (Semrock), and the emission was acquired after 525/50-nm bandpass filter (Semrock). For Voltron2<sub>525</sub>-Kv, M530L4 LED (Thorlabs) was used as the light source, and a filter cube consisting of 520/35-nm bandpass filter (Semrock), 552 nm long-pass dichroic mirror (Semrock), and 572/35-nm bandpass filter (Chroma) was used to collect the fluorescence. For both sensors, the excitation light was set to provide the irradiance of 46 mW/mm<sup>2</sup>. All the images were acquired at 400 fps by using an iXon 860 EMCCD camera (Andor - Oxford instruments). Based on the overlap of the spectra of normalized LED power, excitation filter transmission, and fluorophore excitation, and the overlap of the spectra of fluorophore emission, emission filter transmission, and camera sensitivity, our conditions provided 2.3-fold less efficient excitation (relative to peak excitation) and collection (relative to total emission) of Voltron2<sub>525</sub>-Kv fluorescence compared to ASAP5-Kv at the same irradiance. For the brightness comparison, we used mean intensities in the 0.5–1.5 s time frame due to the rapid decay of fluorescence signals in the first 0.5 s; by bypassing the brighter but highly transient state, we measure the practically usable brightness. Likewise, photostability curves were normalized to values at 0.5 s. To compare the photostability of the two different sensor systems, we used time-lapse images acquired as described above at an irradiance of 46 mW/mm<sup>2</sup>. But as a 2.3-fold lower irradiance of ASAP5-Kv was found to yield the same SNR for mEPSPs as Voltron2<sub>525</sub>-Kv irradiated at 46 mW/mm<sup>2</sup>, we multiplied the time-axis of ASAP5-Kv by 2.3 to produce photobleaching curves at irradiances that provide the same SNR. We also used the difference as correction factor to either add corresponding Gaussian noise to the ASAP5-Kv fluorescence traces or to improve the SNR of Voltron2-Kv detected events by multiplying the square root of 2.3 assuming photon shot noise limited condition.

### Detecting mEPSPs at the soma in cultured neurons

A deconvolution-based method was applied to detect mEPSPs in both electrophysiological and optical recordings of cultured neurons. The electrophysiological recording was first downsampled from 10 kHz to 400 Hz to match the sampling rate of the optical recordings, from which we collected 30 mEPSPs with the highest peak amplitude and averaged the waveforms aligned by their peaks to construct a template. The deconvolution divisor was the repolarizing phase of the template normalized to its peak value. Then we deconvolved the electrophysiological and optical recordings with the divisor, applied a Gaussian filter ( $\sigma=3$ ) to remove the high-frequency noise and a 2 Hz high-pass filter to remove the baseline fluctuation. We identified the peaks in the deconvolved traces with a Z score higher than 2.5 as the detected events. For SNR comparison, the noise was estimated by the standard deviation of the 20 Hz-high-pass-filtered trace to exclude sub-threshold activities in the recording, and the signal was defined by the optical signal corresponding to the detected mEPSPs in the electrophysiological recording.

To detect electrical and optical mEPSPs using miniML, we extracted and labeled events and event-free segments from electrophysiological data using a template-matching algorithm. These annotated data (total segments, 900; label ratio 1:1) were used to

train a machine-learning model for event detection using transfer learning.<sup>29</sup> Corresponding imaging data from both sensors (Voltron2-Kv and ASAP5-Kv; total segments, 800; label ratio 1:1) were used to train a separate model to detect events in the fluorescence traces. mEPSPs in electrophysiological recordings were detected using the electrophysiology-trained miniML model. Fluorescence recordings were filtered using an 8-sample Hann window and then resampled to 4 kHz. Events in the imaging data were detected using the distinct optical model (Figure 5) or the electrophysiology-only trained model (Figure S5).

#### Mapping the propagation of mEPSPs in cultured neurons

Cultured rat cortical neurons at 23 and 24 DIV in extracellular solution containing 145 mM NaCl, 3 mM KCl, 2 mM CaCl<sub>2</sub>, 2 mM MgCl<sub>2</sub>, 10 mM HEPES, and 10 mM glucose (pH adjusted to 7.4) with TTX (1 µM) and PTX (50 µM) were imaged with a sCMOS camera (Flash4-V2 C11440-22CU, Hamamatsu). Excitation light from UHP-F-455 LED (Prizmatix) passed through a 482/18-nm bandpass filter (Semrock) and was focused by a ×40 1.2-NA water-immersion objective lens (Zeiss), and the emission light was collected after a 525/50-nm bandpass filter (Semrock). Neurons were imaged for 13000 frames at 200 fps, with the irradiance of 114 mW/mm<sup>2</sup>. To analyze the images, we first corrected for the rolling-shutter delay of the camera. Then we binned the image by 8×8 to enhance the SNR of single pixels. We generated the masks of neurons by Otsu-thresholding, from which we extracted fluorescence traces from each pixel. We applied 0.5 Hz high-pass filter to detrend the traces and identified peaks with Z scores higher than 3.5 as signals. All peaks were sorted in time, and consecutive peaks within 15 ms were collected and defined as a propagation event. Propagation events that contained less than 5 pixels were removed due to less reliability. For each propagation event, the pixel with the highest peak amplitude was identified as the initiation site of the propagation, and the distance to soma was measured along the dendrite. The somatic trace was pooled from a manually-drawn somatic mask and the signal that corresponds to a propagation was identified according to the averaged peak time of all the signals in a propagation event.

#### Brightness comparison in cultured neurons

Hippocampal neurons were transfected at 9–11 DIV with 200 ng of indicator DNA (pAAV-hSyn-ASAP-Kv-mCyRFP3) and 1 µL of Lipofectamine 2000 (Thermo Fisher Scientific) in 200 µL of Neurobasal with 2 mM GlutaMAX and imaged 2 d after transfection. Neurons were imaged on an inverted microscope (Zeiss Axiovert 200M) with a ×40 1.2-NA objective (Zeiss). Excitation light was 488/30-nm filtered from a 120-W mercury vapor short arc lamp (X-Cite 120PC, Exfo). Fluorescence was collected using a 531/40-nm filter (for green channel) and a 625/60-nm filter (for red channel). Images were taken using an Orca Flash4.0LT+ C11440-42U CMOS camera (Hamamatsu) with µManager software.

#### One-photon voltage imaging in mouse and sensor comparison

##### Surgery and viral injection

To prepare mice for both one- and two-photon *in vivo* imaging from primary motor cortex, we followed the procedure previously described<sup>9,52</sup> with a few modifications. Briefly, 8–14 weeks-old wild-type C57BL/6J mice (Jackson Laboratories, No. 000664) of both genders were injected with relevant GEVI viruses (floxed versions of ASAP3-Kv, JEDI-1P-Kv, JEDI-2P-Kv, and ASAP5-Kv under the EF1a promoter) mixed with diluted CaMKIIα Cre virus ( $2.8 \times 10^{13}$  GC/mL, Addgene #105558). All four GEVI viruses were produced by the Stanford GVVC in the same batch, but for a better comparison, we further diluted higher titer viruses to match with the lowest titer one which had the titer of  $4.59 \times 10^{12}$  vg/mL. For each mouse, 450 nL of the GEVI virus was mixed with 50 nL of CaMKIIα Cre virus pre-diluted for 100 times in volume to make the GEVI virus (floxed) to diluted CaMKIIα Cre virus ratio to be 148:1 in terms of virus particles. The intracranial virus injection was done on the left hemisphere at the coordinate; ML –1.5 mm, AP 1.0 mm, and DV 1.2–1.0 mm (all measured from bregma), for sparse labeling of layer 2/3 pyramidal neurons in motor cortex. Cranial window surgery was done either directly following the injection or 3–4 weeks after the injection. We did not see noticeable difference in expression or cranial window quality between the two groups. In brief, a 3×3-mm craniotomy was cut using #11 scalpel blades (Fine Science Tools) and a square coverslip (#1 coverslip glass, Warner Instruments) was implanted on top of the dura within the craniotomy with mild compression of the brain. The window was centered at ML –2.0 mm, AP 0.5 mm. The window was sealed to the skull using dental cement (C&B Metabond, Parkell) and at the end of surgery, a custom titanium headplate was attached to the skull to fixate the head to the microscope stage during subsequent imaging. Once the animals recovered, and the window and head-plate stayed in good quality, all the mice were made blind to the experimenter by another researcher. The experimenters were left blind for the identity of each animal until all one-photon *in vivo* imaging and analyses were done. The identity was only revealed for the statistical comparison between GEVI groups.

##### One-photon *in vivo* imaging and analysis

The one-photon wide-field voltage imaging setup was similar to what was previously described.<sup>9</sup> Briefly, a BX-51 microscope (Olympus) equipped with a 470-nm LED (SOLIS-470C, Thorlabs), a long-working distance ×20 objective lens (NA 1.0, Olympus), a Flash4.0 V2 scientific CMOS (sCMOS) camera (C11440-22CA, Hamamatsu), and a FITC-5050A filter set (Semrock) was used. High-speed acquisition of fluorescence images at 500 fps was achieved by reading 64 vertical lines from the 4×4-binned sCMOS sensor. Light intensity was 50 mW/mm<sup>2</sup> for all animals. Resulting images were converted to TIF files and corrected for lateral motion using turboReg<sup>53</sup> (<https://imagej.net/plugins/turboreg>). The ROIs for neurons and background were selected using a customized program in MATLAB (Mathworks). Then the fluorescence trace was extracted from the TIF files (as the average signal in each ROI, unless otherwise specified), background-subtracted, and photobleaching-corrected for spike detection and quantification in

customized Python program. To correct for photobleaching, a piece-wise step function with 0.5-s window size was used to fit the fluorescence trace to estimate the baseline. In each 0.5-s window, the baseline was the average of the 30–80 percentile of the fluorescence values, to exclude extreme values and signals. Spike location was determined using the spikepursuit algorithm in Volpy.<sup>50</sup> For brightness comparison, background subtracted fluorescence intensity during the first second of each cellular ROI was averaged over time and compared. For SNR comparison, the noise was estimated by the standard deviation of the 20 Hz-high-pass-filtered and spike-removed trace, to exclude supra- and sub-threshold activities in the recording, and the signal was defined by the peak value of the spikes. The Python programs for data processing can be find in our GitHub repository (<https://github.com/AlexYkHao/spikenotes.git>).

#### Confocal imaging of brain slices

To evaluate sparse GEVI expression in motor cortex after one-photon *in vivo* voltage imaging, the brain was sliced and imaged as previously described.<sup>52</sup> Briefly, mice were anesthetized with isoflurane and fixed with 4% paraformaldehyde in phosphate-buffered saline (PBS) by transcardiac perfusion. After craniotomy, the brain was dissected out and then further fixed in 4% PFA/PBS in room temperature for 1–2 h, and then further incubated in 4°C for 24 h. The brain was transferred to 30% sucrose/PBS solution for at least 3 days. The fixed brain was frozen and sliced into 50-μm thick coronal sections using a sliding microtome (Leica). The brain slices were mounted on a slide glass in DAPI containing mounting media (VectaShield H-1500, Vector Laboratories). The slide was imaged using a confocal microscope (LSM900, Zeiss).

#### One-photon voltage imaging in zebrafish

The genotypes of the GEVI-expressing zebrafish are HuC:Gal4; 10×UAS:ASAP3-Kv for ASAP3, and HuC:Gal4; 10×UAS:ASAP5-Kv for ASAP5. Zebrafish was imaged on day 4 post transfection, using a ×20 1.0-NA objective (Olympus) with a magnification ratio of 22.22. A 473 nm blue laser was used as an excitation light source, with light-sheet intensity to be ~1000 mW/mm<sup>2</sup>. The videos were recorded using a Hamamatsu ORCA-Flash4.0 v3 camera, with 3.32 ms exposure time. All procedures related to zebrafish husbandry and handling were conducted in accordance with the US National Institutes of Health Guide for the Care and Use of Laboratory Animals and approved by the MIT Committee on Animal Care.

#### Two-photon *in vivo* imaging of *Drosophila*

Female flies, 5 days post eclosion, were mounted, dissected to expose the brain, and perfused with an oxygenated saline-sugar solution during imaging, following standard methods.<sup>18</sup> For Mi1 and L2, a 920 nm laser beam with 25 mW of post-objective power excited the fluorophores, and photons were collected with a 525/50-nm filter. Data was collected at a frame rate of 354 fps and a resolution of 0.265 μm in X and Y using a resonant-galvanometric scanning microscope (Bruker) with a ×20 1.0-NA objective (Leica).

Visual stimuli were generated as previously described.<sup>54</sup> Briefly, two projectors (Lightcrafter 4500, Texas Instruments) with a 482/18-nm filter generated visual stimuli at 120 Hz. A photodiode (Thorlabs, SM05PD1A) was used to align the timing of the stimulus to image acquisition. Visual stimuli were full-field 24-ms contrast increments and decrements (50 presentations each, in random order), interleaved in time by 500 ms presentations of gray. Images were motion-corrected using turboReg.<sup>53</sup> Background was subtracted for each resonant-galvanometric scanning line before analysis. To do this, 20 contingent pixels with the lowest brightness value were averaged to calculate the background value for each scanning line. The extracted fluorescence traces were filtered by 120 Hz-band-pass filter to further remove bleed-through photons from the projectors with 120 Hz refresh rate. The peak response (peak ΔF/F) was computed by identifying the ΔF/F value farthest from zero in the expected direction (depending on the stimulus), and the time to peak (*t*<sub>peak</sub>) was the time of this response relative to the start of the contrast change. For calculating SNR, the noise was estimated by the standard deviation of the signal in the 100 ms window before the onset of the visual stimulus, and the signal was defined by the peak value of the stimulus-triggered optical signal.

For the TPN-II neuron, when imaged using the resonant scanning microscope (Bruker), a 920 nm laser beam with 25 mW of post-objective power was used and data was collected at 779 fps and 0.38 μm x-y resolution using a resonant-galvanometric scanning microscope (Bruker) with a ×20 1.0-NA objective (Leica). On one AOD microscope (Karthala) a 920 nm laser beam with 25 mW of post-objective power was used and data was collected at 3333 fps using a ×25 1.1-NA objective (Nikon). To simultaneously image two TPN-II neurons in the same brain, a second 3D AOD microscope (Femtonics) with 25 mW of post-objective power was used and data was collected at 3288 fps using a ×25 1.1-NA objective (Nikon). For calculating SNR, the noise was estimated by the standard deviation of the 20 Hz-high-pass-filtered and spike-removed trace, to exclude supra- and sub-threshold activities in the recording, and the signal was defined by the peak value of the spikes.

#### Two-photon *in vivo* voltage imaging in mouse motor cortex

##### Resonant-galvanometric two-photon voltage imaging

Two-photon imaging in motor cortex was performed in the same mice used for one-photon *in vivo* imaging in mouse motor cortex. Following surgery and one-photon imaging (described under “[one-photon voltage imaging in mouse and sensor comparison](#)”), images were acquired using a custom-built two-photon microscope system with a resonant scanner (LotosScan, Suzhou Institute of Biomedical Engineering and Technology) and a ×25 / 1.0 NA water immersion objective lens (Olympus). A mode-locked tunable ultrafast laser (InSightX3, Spectra-Physics) at 925 nm was used for imaging with a post-objective power of 30–160 mW.

A 240×48-pixel field of view was imaged at 500 fps using a pixel size of 0.6  $\mu\text{m}$  in X and 1.0  $\mu\text{m}$  in Y. Resulting images were exported in TIF files and analyzed in the same pipeline as described in the one-photon imaging method session.

#### **Three-dimensional in vivo random access two-photon voltage imaging**

For the 3D random-access two-photon voltage imaging, we used Femto 3D Atlas Plug & Play microscope which was made portable for demonstration purposes by Femtonics (Hungary). This portable stand-alone rig was equipped with a 920 nm fiber-laser and acousto-optic crystals for random-access two-photon volumetric excitation through a  $\times 16$  0.80-NA long-working distance objective lens (Nikon). The post-objective laser power was 25 mW.

During imaging, a mouse sparsely expressing ASAP5-Kv in motor cortex in CaMKII $\alpha$ -positive neurons was head-fixed to the custom-made head-post and run on a running wheel device modified to fit onto the demo scope's specimen stage. The running was recorded by a running encoder and the mouse motion was imaged using an infrared-camera for the duration of imaging. Resulting images were exported in TIF files and fluorescence traces were extracted using a customized Python program.

#### **Two-photon *in vivo* voltage imaging in mouse visual cortex in behaving mice**

##### **Viral injections and surgeries**

AAV9-EF1-DIO-ASAP5-Kv viruses were injected at a titer of  $3 \times 10^{12}$  vg/ml and AAV2/1 hSyn-Cre (Addgene, AV-1-PV2676) was co-injected at a final titer of  $2.10^9$  GC/ml. Viruses were combined in a saline solution containing 0.001% of pluronic acid (ThermoFischer 24040032), 300 nl of which was injected at a flow rate of 75 nl/min into the visual cortex (V1 coordinates from bregma: anteroposterior -3/-3.5 mm, mediolateral -2.5/-3 mm, and dorsoventral -0.3 mm from brain surface). A custom-designed aluminum head-plate was fixed on the skull with layers of dental cement (Metabond). A 5-mm diameter #1 coverslip was placed on top of the visual cortex and secured with dental cement (Tetric evoflow). Mice were allowed to recover for at least 15 days before recording sessions and housed at least 2 mice per cage. Behavioral habituation was adopted, involving progressive handling by the experimenter with gradual increases in head fixation duration.<sup>55</sup> Mice were handled before recording sessions to limit restraint-associated stress, and experiments were performed during the light cycle.

##### **ULoVE voltage optical recording and experimental design**

1-3 h recording sessions were performed while mice behaved spontaneously on top of an unconstrained running wheel in the dark.<sup>55</sup> Recordings were performed using a custom designed acousto-optic deflectors (AOD)-based random-access multiphoton system (Karthala System) based on a previously described design.<sup>14</sup> The excitation was provided by a femtosecond laser (InSight X3, Spectra Physics) mode-locked at 920 with a repetition rate of 80 MHz.

A water-immersion objective (CFO Apo25XC W1300, 1.1 NA, 2 mm working distance, Nikon) was used for excitation and epifluorescence light collection. The signal was passed through an IR blocking filter (TF1, Thorlabs), split into two channels using a 562 nm dichroic mirror (Semrock), and passed to two H12056P-40 photomultiplier tubes (Hamamatsu) used in photon counting mode. The 510/84-nm filtered green channel was used for collecting ASAP5 signals. The optimized ULoVE excitation pattern (unpublished data) consists of a series of 9 points vertically aligned (evenly spread over a distance of 15  $\mu\text{m}$ ), multiplexed twice horizontally with a 2  $\mu\text{m}$  spacing. The 18 points are scanned in diagonal (8  $\mu\text{m}$  horizontally and 3  $\mu\text{m}$  vertically) during the acquisition time of 50  $\mu\text{s}$ , in order to homogeneously fill an extended excitation volume continually encompassing the cell plasma-membrane. This latest strategy refines the axial profile of excitation, limiting signals out of the desired focal plane, thus reducing any neuropil signal contamination and improving SNR. For imaging, laser power was set to deliver 15 mW post-objective and pre-sample then adjusted for mono-exponential loss through tissue with a length constant of 170 mm. For ULoVE optical recordings, we further multiplied the power by 1.5, compared with the applied power used in the imaging mode, to account for the greater excitation volume. The applied power never exceeded 200 mW. Using two patterns per cell enabled a temporal resolution of 7142.9 Hz. Recordings were stopped after 320 s. For recording, we selected neurons that were sufficiently bright to obtain significant signal-to-noise, yet did not display long lasting depolarizing plateaus, indicative (in our observations) of over-expression. Cell depth measured from the surface of the brain was 100–230  $\mu\text{m}$ .

##### **Signal analyses, spikes extraction, and waveform analyses**

Photobleaching was assessed by bi-exponential fitting and corrected by division of the raw trace by the normalized fit function. After removing the remaining low frequency drift using a zero-phase distortion filter (high pass: 0.5 Hz), the trace was converted to %  $\Delta F/F_0$  taking the mean signal as  $F_0$ . Spikes were detected with a custom designed algorithm, which utilizes three metrics to sort aspects of spike shape and threshold, all of them with Z scores above 3. The first metric is to high pass filter the trace (second order Butterworth filter with lower limit set at 40 Hz). The second metric is a cumulative probability transformation of the signal using the standard erf function for a duration of 1.6 ms. The third metric takes the cumulative product of the 2<sup>nd</sup> to the 5<sup>th</sup> scale of the coif1 discrete wavelet transform and applies a global realignment to retrieve energy in various frequency bands in one peak. To extract the spike waveform metrics, an average spike waveform was aligned on the spike onset. Then spike amplitude was taken as the peak value of the spike waveform average, measured from the onset point. FWHM corresponds to the extent in time at half maximum amplitude, taken from the average spike waveform after 20 kHz linear interpolation. To quantify subthreshold fluctuations, traces were filtered using a bidirectional Butterworth bandpass filter between 0.1 and 30 Hz. The cell up state corresponds to the mean signal within 5ms surrounding detected spikes, and the cell down state corresponds the 1<sup>st</sup> percentile of that filtered trace. The subthreshold fluctuation is taken as the difference between the cell up and the cell down states.

## Two-photon *in vivo* imaging in barrel cortex

### Surgery and viral injection

Mice aged 2 to 3 months old were anesthetized with isoflurane (1.0–1.5% in O<sub>2</sub>). C1, C2 and C3 whisker columns were localized using transcranial intrinsic signal optical imaging to target the viral injections. A 3-mm diameter craniotomy was made centered on the C2 column.<sup>56</sup> AA9-hSyn-ASAP5-kv was injected at 5–6 locations surrounding the C2 column at 250 µm and 350 µm depth. A chronic cranial window (3-mm diameter glass coverslip, #1 thickness, CS-3R, Warner Instrument) was attached with dental cement after viral injections. Before surgery, mice received dexamethasone (2 mg/kg), enrofloxacin (5 mg/kg), and meloxicam (10 mg/kg). Buprenorphine (0.1 mg/kg) was administered as the post-operative analgesic.

### Behavioral task

Mice were acclimated to head-fixation and the imaging rig across 4 days prior to data collection. At the start of each imaging session, mice were anesthetized with isoflurane and head-fixed under the two-photon microscope. 9 whiskers (rows B-D, arcs 1-3) were inserted into a 3×3 array of small tubes with calibrated piezoelectric actuators, centered on the C2 whisker. After mice recovered from anesthesia, trials consisted of 16×200-µm single whisker deflections were applied 5 mm from the face with 500-ms spacing between stimuli. Individual whisker stimuli were delivered in random order with equal probability. An inter-trial interval of 2 ± 0.5 s was used between trials. Approximately 80 trials were delivered over the course of 15 min imaging. Paw guards prevented paw contact with the piezos. Imaging experiments were performed in total darkness and mouse activity was tracked using 850 nm IR illumination and a high-speed tracking camera. Uniform white noise was continuously applied to mask sounds from piezo actuators. Stimulus delivery was controlled by an Arduino Mega 2560 and custom routines in Igor Pro (WaveMetrics).

### Two-photon imaging

Two-photon imaging took place 3–4 weeks after viral injection on awake head-fixed mice. Imaging was performed with a modified, commercially available (ThorLabs) two-photon microscope.<sup>57</sup> A titanium-sapphire laser (Chameleon Ultra II, Coherent) was used as the two-photon excitation source, and a wavelength of 960 nm was used to excite ASAP5-Kv. A post-objective power of 30–50 mW was used for imaging at depths of 160–200 µm below brain surface. 512×32-pixel fields of view were imaged using a pixel size of 0.625 µm per pixel, resulting in a 310×20-µm area imaged at 397 fps.

### Image processing

Fluorescence images were corrected for x-y motion using NoRMCorre.<sup>58</sup> Neuronal regions of interests (ROIs) were manually annotated using ImageJ (NIH) based on the mean intensity image.  $\Delta F/F_0$  traces were extracted, with  $F_0$  defined as the peak of fluorescence histogram of the ROI across each 15-min movie. Spike locations and subthreshold activity were extracted using the CalmAn algorithm<sup>59</sup> and custom Python routines (available at the SpkXtract Github repository) unless otherwise stated. The total number of imaged neurons across the three fields of view in Figure 4 were  $n = 36$ .

### Whisker-evoked responses and receptive field analysis

To identify neurons with significant whisker responses, we used a permutation test comparing the difference in spike number in a 50 ms post-stim period relative to a pre-stim period of the same length for each whisker stimulus. In each iteration of the permutation test, single-trial extracted spike number were randomly shuffled between the post-stimulus period and the pre-stimulus period, and the difference in response between these shuffled trial sets was calculated. This was repeated 10,000 times to generate a null distribution. A given whisker response was considered significant if it exceeded the 95th percentile of this null distribution.  $p$  values were corrected for multiple comparisons across all whisker stimuli using a false discovery rate of 0.05. A neuron was considered whisker-responsive if one or more whisker stimuli resulted in a significant spiking response. In our dataset, 77.8% of cells exhibited at least one significant spiking response to a whisker stimulus.

## QUANTIFICATION AND STATISTICAL ANALYSIS

Statistical analyses were performed in Prism 10 (GraphPad). Specifically, distributions were first checked for normality by the Kolmogorov-Smirnov test. For comparisons of two groups, unpaired t tests were performed for normally distributed data, and Mann-Whitney tests for nonparametric data. For comparisons of more than two groups, one-way analysis-of-variance (ANOVA) followed by pairwise t tests with Bonferroni corrections was performed for normally distributed data. For nonparametric data, Kruskal-Wallis tests followed by Dunn's multiple-comparisons tests was used. The statistical details of experiments can be found in the figure legends. The  $p$  values are all listed in the figures, and we used  $p < 0.05$  as a threshold for statistical significance when describing the results.